Mooberry, E. S., and Krugh, T. R. (1975), *J. Magn. Reson. 17,* 128.
Newmark, R. A., and Cantor, C. R. (1968), *J. Am. Chem. Soc. 90,* 5010.
Patel, D. J., and Tonelli, A. E. (1974), *Biopolymers 13,* 1943.
Pitha, J., Jones, R. N., and Pithova, P. (1966), *can. J. Chem. 44,* 1045.
Raszka, M., and Kaplan, N. O. (1972), *Proc. Natl. Acad. Sci. U.S.A. 69,* 2025.
Shoup, R. R., Miles, H. T., and Becker, E. D. (1966), *Biochem. Biophys. Res. Commun. 23,* 194.
Sobell, H. M. (1969), *Genet. Organ. 1,* 91.
Ts'o, P. O. P. (1974a), in Basic Principles in Nucleic Acid Chemistry, Vol. I, Ts'o, P. O. P., Ed., New York, N.Y., Academic Press, p 453.
Ts'o, P. O. P. (1974b), in Basic Principles in Nucleic Acid Chemistry, Vol. II, Ts'o, P. O. P., Ed., New York, N.Y., Academic Press, p 305.
Ts'o, P. O. P., Kondo, N. S., Schweizer, M. P., and Hollis, D. P. (1969), *Biochemistry 8,* 997.
Van Geet, A. L. (1970), *Anal. Chem. 42,* 679.

Conformation and Interaction of Short Nucleic Acid Double-Stranded Helices. I. Proton Magnetic Resonance Studies on the Nonexchangeable Protons of Ribosyl ApApGpCpUpU†

Philip N. Borer, Lou S. Kan, and Paul O. P. Ts'o*

ABSTRACT: ^1H nuclear magnetic resonance (NMR) spectra of a self-complementary ribosyl hexanucleotide, A_2GCU_2, are investigated as a function of temperature and ionic strength in D_2O. Seventeen nonexchangeable base and ribose-$H_{1'}$ resonances are resolved, and unequivocally assigned by a systematic comparison with the spectra of a series of oligonucleotide fragments of the A_2GCU_2 sequence varying in chain length from 2 to 5. Changes in the chemical shifts of the 17 protons from the hexamer as well as the six $H_{1'}$-$H_{2'}$ coupling constants are followed throughout a thermally induced helix-coil transition. These δ vs. T and J vs. T (°C) profiles indicate that the transition is not totally cooperative and that substantial populations of partially bonded structures must exist at intermediate temperatures, with the central G·C region being most stable. Transitions in chemical shift for protons in the same base pair exhibit considerable differences in their T_m values as the data reflect both thermodynamic and local magnetic field effects in the structural transition, which are not readily separable. However, an average of the T_m values agrees well with the value predicted from studies of the thermally induced transition made by optical methods. The values of $J_{1'-2'}$ for all six residues become very small (<1.5 Hz) at low temperatures indicating that $C_{3'}$-endo is the most heavily populated furanose conformation in the helix. The δ values of protons in the duplex were compared with those calculated from the ring current magnetic anisotropies of nearest and next-nearest neighboring bases using the geometrical parameters of the A′-RNA and B-DNA models. The δ values of the base protons in the duplex calculated assuming the A′-RNA geometry agree (±~0.1 ppm) with the observed values much more accurately than those calculated on the basis of B-DNA geometry. The measured δ values of the $H_{1'}$ are not accurately predicted from either model. The synthesis of 35 mg of A_2GCU_2 using primer-dependent polynucleotide phosphorylase is described in detail with extensive discussion in the microfilm edition.

In recent years extensive studies have been made of the physical properties of oligoribonucleotides of defined sequence which are capable of double helix formation. The investigations dealt with the structure of these molecules in solution as well as the thermodynamics and kinetics of their helix-coil transition. The pioneering studies of Martin, Uhlenbeck, and Doty (Martin et al., 1971; Uhlenbeck et al., 1971) provided thermodynamic information from the hypochromicity as a function of temperature for several double helical oligomers. These papers also outlined the enzymatic procedure for the "block copolymerization" of such oligonucleotides, whose sequences were designed to favor the formation of perfect double helices. This obviated the problems of triplex formation and other states of high agregation encountered by previous workers.

Subsequent studies have substantially extended the understanding of the structure and stability of these oligomer helices in solution. Borer et al. (1974b) have reported thermodynamic parameters for 19 RNA duplexes of chain length 6–14 based on their hypochromicity as a function of

† From the Division of Biophysics, School of Hygiene and Public Health, The Johns Hopkins University, Baltimore, Maryland 21205. *Received January 30, 1975.* This work was supported in part by a grant from the National Institutes of Health (GM016066-06, 07) and a grant from the National Science Foundation (GB-30725x). Experiments with the 220-MHz instrument were performed at the NMR Regional Facilities Center at the University of Pennsylvania, established by National Institutes of Health Research Grant No. 1P07RR-00542-01 from the Division of Research Facilities and Resources. P.N.B. (1973–1975) and L.S.K. (1972–1974) have received National Institutes of Health Postdoctoral Fellowships.

temperature. Several workers have examined the temperature-jump relaxation kinetics of the helix–coil transition in these molecules. Craig et al. (1971), Pörschke et al. (1973), Gralla and Crothers (1973a,b), and Ravetch et al. (1974) showed that molecules designed to form duplexes had relaxation characteristics most easily interpreted in terms of a dimerization process. Additionally, Gralla and Crothers (1973a) examined the kinetics of association of the $A_4GC_nU_4$ series where the oligomers with $n > 1$ form helices with mismatched bases. Their study included a classic analysis of sedimentation equilibrium experiments which showed the oligomers with $n \geq 5$ formed unimolecular "hairpin" loops while those with $n \leq 4$ formed bimolecular complexes (strand concentrations for these studies were $\sim 10\ \mu M$).

The self-complementary A_mGCU_m series (m = 2–5) has been the subject of thermodynamic investigations in three laboratories. Uhlenbeck and Borer (Borer et al., 1974b) synthesized the oligomers and studied their A_{260} vs. T (°C) profiles in 1 M NaCl. Pörschke et al. (1973) used T-jump relaxation methods to examine the optical transition of several oligomers prepared by Uhlenbeck and Borer. Ravetch et al. (1974) independently studied the thermodynamic and kinetic parameters for this oligomer series by T-jump relaxation methods. Their data on A_4GCU_4 and A_3GCU_3 agree well with the aforementioned studies. However, their examination of A_2GCU_2 showed a transition with an aberrantly low T_m and large breadth when compared to the other two studies or an extrapolation of their own data on the longer helices. The apparent resolution of the matter was discovered when the latter group examined the separation and identification procedures used to characterize their sample of A_2GCU_2. Their sample probably contained an oligomer of incorrect chain length or sequence (D. M. Crothers, private communication). The important question raised by the Ravetch et al. article remains unanswered: really how suitable are short oligonucleotides as models for longer regions in natural nucleic acids? The question probably cannot be answered at the level of the experiments described and will not be until careful systematic studies are carried out with experimental probes at atomic resolution using nuclear magnetic resonance (NMR) or Raman techniques.

The study of oligomeric duplexes of nucleic acids by NMR promises to be a particularly fruitful approach to examining their detailed structure in aqueous solution. It should be possible to resolve and assign most of the base and sugar-$H_{1'}$ resonances in oligomers of ten bases or less and draw conclusions about the local environment of each. Furthermore, it has been observed that long double helical nucleic acids cannot be studied because their rigidity and length do not allow them to exhibit rapid segmental motion or tumbling in solution (McTague et al., 1964, McDonald et al., 1964, 1967). The consequence of this loss of motion is severe dipolar broadening of the resonance lines.

Lubas and Wilczok (1971) determined the overall correlation time, τ_c, of helical DNA to be $\sim 10^{-8}$ sec. This would correspond to a $T_2 \simeq 3 \times 10^{-4}$ sec (Bovey, 1969) and a line width of ~1000 Hz, far too broad to observe in high-resolution NMR. This overall correlation time should represent an upper limit for a segment of a long, rigid helix. The magnetic dipoles have many more orientations with respect to the applied field direction in flexible or short nucleic acid helices. Thus, "motional averaging" (Bovey, 1969) in segmental movement or in tumbling reduces the resonance line width. An affective τ_c in the range of 10^{-10}–10^{-11} sec should allow the oligomers to have narrow enough resonance lines (3–30 Hz) for high-resolution spectra.

Cross and Crothers (1971) analyzed the ^1H NMR spectrum of an oligo-DNA duplex, dTTGTT·dAACAA. Only the thymine methyl resonances could be followed throughout the helix–coil transition, however, as the other lines were still very broad in the duplex. The reason for this broadening is not clear. When the present work was nearly completed, Heller et al. (1974) reported ^1H NMR spectra of a $rA_{20\text{-}25}$·$rU_{20\text{-}25}$ complex. The lines of the nonexchangeable protons were separable into groups corresponding to the H_2, H_8, and H_6 protons, but could not be dissected into resonances from the individual bases. In a recent series of articles, Patel and Tonelli (e.g., Patel and Tonelli, 1974) reported the investigation of the NH–N protons of several short self-complementary DNA helices. Also, Arter et al. (1974) have recently published well-resolved spectra of the N–H and C–H protons of rCCGG.

In this communication we report the measurement and assignment of 17 base C–H and ribose C–$H_{1'}$ resonances of self-complementary A_2GCU_2 throughout a thermally induced helix–coil transition at three ionic strengths. The observed chemical shifts and coupling constants of the $H_{1'}$ resonances have been compared with those predicted from the A′-RNA and B-DNA models. In the following paper (Kan et al., 1975a), we report the ^1H NMR of the three unique exchangeable hydrogen-bonded NH–N protons of this helical duplex, $(A_2GCU_2)_2$. Preliminary reports of the ^1H NMR of this molecule have been presented previously (Borer et al., 1974a; Ts'o et al., 1975).

Results

General Characteristics of the Base and Ribose-$H_{1'}$ NMR Spectra. Figure 1 shows 220-MHz ^1H NMR spectra of 10 mM A_2GCU_2 at four temperatures from 76.5 to 5°C in 0.17 M Na^+. The lowest field group of eight resonances (at the left of the figure) are the purine H_8 and adenine H_2 singlets and pyrimidine H_6 doublets. The nine doublets at higher field are the pyrimidine H_5 and ribose $H_{1'}$ resonances. Figure 2 focuses on the H_2, H_8, H_6 group with 220-MHz spectra in 0.07 M Na^+ in Figure 2a and 100-MHz spectra in 1.07 M Na^+ in Figure 2b.

Three general features characterize these spectra: (1) The resonance lines are narrow at high temperature and broad at low temperature. This consequence of the decrease in segmental motion at low temperature is also reflected in the number of pulses necessary to acquire spectra of acceptable signal-to-noise ratio. The Fourier transform operation required 50 pulses for the highest temperature spectrum of Figure 1 while 1000 pulses were necessary for the lowest temperature spectrum. (2) There are dramatic, predominantly upfield, changes in the chemical shifts of these reso-

[1] Abbreviations used are: A_2GCU_2, ribosyl ApApGpCpUpU (the standard 3′–5′ phosphodiester linkage is implied in the notation for this and other oligoribonucleotides, terminal phosphates are specifically denoted, when present, by a pre- or suffixed p, terminal 2′–3′ cyclic phosphates by a suffixed p>); P_i, inorganic orthophosphate; C_s, concentration of single strands; DSS, 2,2-dimethyl-2-silapentane-5-sulfonate; DEAE-Seph, diethylaminoethyl-Sephadex A-25; PEI-cellulose, polyethylenimine-cellulose; TEA-HCO_3, triethylammonium bicarbonate; RNase T_1, ribonuclease T_1 (*Aspergillus oryzae*, EC 2.7.7.16); RNase A, bovine pancreatic ribonuclease (EC 2.7.7.16); BAPase, bacterial alkaline phosphatase (*Escherichia coli*, EC 3.1.3.1); PNPase, primer-independent polynucleotide phosphorylase (*Micrococcus luteus*, EC 2.7.7.8); PD PNPase, primer-dependent polynucleotide phosphorylase.

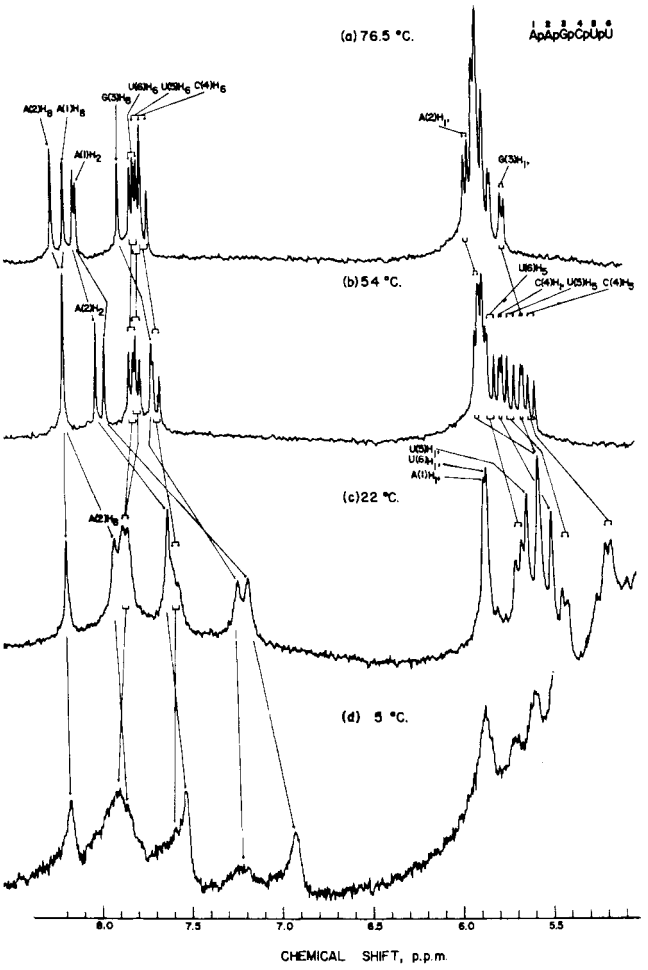

FIGURE 1: The 220-MHz ^1H NMR spectrum of the base and $H_{1'}$ protons of A_2GCU_2. The sample was 10 mM in strands, 0.17 M Na^+, pD 7.0 in D_2O. Chemical shifts were measured in reference to internal t-butyl alcohol and were converted to values with DSS as general standard.

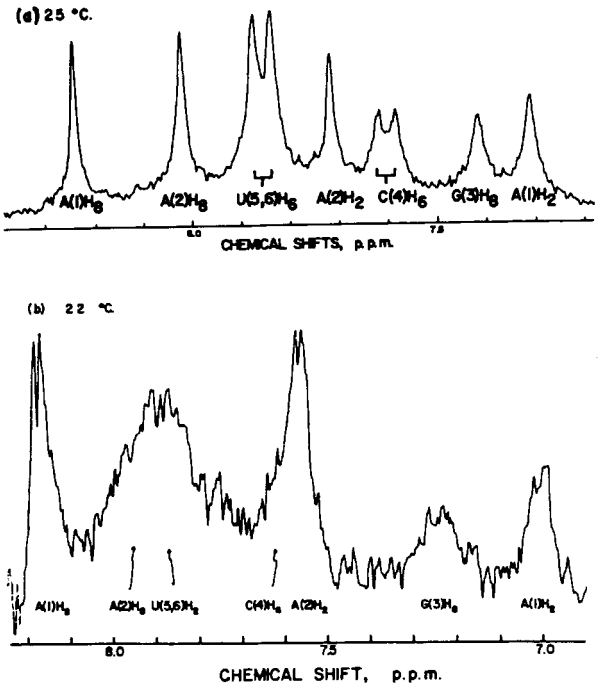

FIGURE 2: Spectra of the H_2, H_6, and H_8 protons of A_2GCU_2 at (a) 220 MHz, 25°C, and (b) 100 MHz, 22°C. The samples were 10 mM in strands, 1.07 M Na^+, pD 7.0 in D_2O. Chemical shifts were referenced to DSS as in Figure 1.

nances upon lowering the temperature. This reflects a large increase in the shielding effects due to the stacking of the bases, especially the purines. (3) There is also an abrupt decrease of the $H_{1'-2'}$ coupling constants upon lowering the temperature. This indicates a change in the conformations for the furanose rings. All these observations are consistent with the notion that A_2GCU_2 assumes an ordered structure at sufficiently low temperatures.

At high temperatures, the H_2, H_8, and H_6 resonances are well resolved; while the H_5 and $H_{1'}$ resonances are better separated at intermediate temperatures (20–50°C, Figure 1). At low temperatures, the H_2, H_8, and H_6 resonances are still sufficiently well resolved for accurate measurement of chemical shifts. However, the $H_{1'}$ and H_5 resonances are partially obscured by the intense HOD peak which shifts downfield due to hydrogen bonding upon decreasing the temperature.

Assignment of the Resonances. Several general considerations allow the assignment of a particular resonance to a certain class. These well-known principles are the following: (1) The chemical shifts of the protons in the oligonucleotides at high temperature closely resemble those of the mononucleotides. (2) The H_5 and H_6 doublets from the pyrimidines have temperature-invariant coupling constants with $J_{5,6}$ values of 7.6 Hz for C and 8.1 Hz for U. The H_5 resonances and the H_6 resonances are separated by about 1.8 ppm with the H_5 resonances located upfield in the region of the $H_{1'}$ resonances. (3) The $H_{1'}$ resonances have temperature-sensitive coupling constants, $J_{1'-2'}$, which are less than 6 Hz and are further reduced at low temperatures. (4) The H_2 and the H_8 singlets can be unambiguously distinguished on the basis of their spin–lattice relaxation time, T_1. The T_1 (5–7 sec) of H_2 is longer than the T_1 (1–3 sec) of H_8 (Ts'o et al., 1973). Therefore, if the 90° pulse rate is increased in the FT mode for spectrum acquisition, the signal intensity of the H_2 resonance decreases faster than the other resonances which all have much shorter T_1 values (Ts'o et al., 1973). (5) A comparison between a 220-MHz spectrum and a 100-MHz spectrum particularly from the same sample under nearly identical conditions is often helpful to differentiate chemical shift effects vs. coupling constant effects on the resonances.

Once the resonances are grouped into classes by the general considerations, the assignments of individual resonances to specific protons is accomplished by a set of three interlocking procedures analyzing the effect on the spectra of a series of oligonucleotides of systematic variations in (1) chain length, (2) temperature, and (3) ionic strength.

The first aspect of this procedure compares the spectra of a sequence related series of oligonucleotides in which each member of the series is incremented one nucleotide unit from its predecessor. Hence, this aspect is termed "incremental assignment". The shortest member of this series must be previously assigned by other standard methods and the longest member is obviously the molecule of interest. In the present case, ApA, A_2G, A_2GC, A_2GCU, and A_2GCU_2 comprise the series. The unambiguous assignment of the ApA resonances was made by Kondo and Danyluk (1972) who selectively deuterated the dimer. The spectra of the series of oligomers are usually recorded in low salt, at high temperature, and, if possible, at low strand concentration. In this environment the inter- and intrastrand interactions

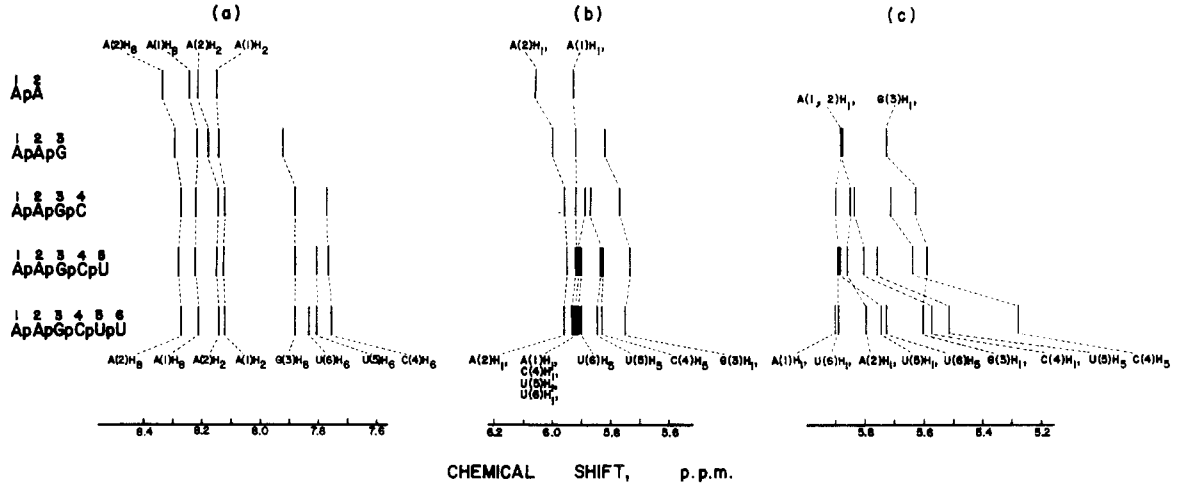

FIGURE 3: The incremental assignment scheme for all the base and $H_{1'}$ resonances of A_2GCU_2. The thickness of the lines represents the number of signals contained in a resonance envelope. (a) The assignment of H_2, H_6, and H_8 resonances at ~65°C. (b) The assignment of $H_{1'}$ and H_5 resonances at ~65°C. Four resonances are clustered at this temperature. (c) The assignment of $H_{1'}$ and H_5 resonances at ~35°C. The four resonances clustered at ~65°C are resolved at this temperature and can now be assigned. $[Na^+] = 0.02\ M$ and $C_s = 1$ mM for each of the spectra except for the hexamer spectrum shown in the 5–6-ppm region (Figure 3b,c) where $C_s = 10$ mM and $[Na^+] = 0.07\ M$. Chemical shifts are expressed in reference to DSS.

are greatly reduced as indicated by the similarity of the oligomer and monomer spectra, also the resonances are narrow and usually better resolved. Each of the oligomers in the series exists as a substantially unstacked single strand; therefore, any major change in the resonance pattern from an oligomer to the one incrementally longer is due to the resonances of the new nucleotide and its shielding effects on the previously present protons. The magnetic field effect of the newly added nucleotide acts principally on its immediate 5′-neighbor. This incremental comparison for the A_2GCU_2 series is displayed in Figure 3. The eight resonances in the 7–8-ppm region shown in Figure 3 are simple and unambiguously assigned using this procedure.

The second aspect of the assignment procedure compares the effect of temperature variations as demonstrated in Figure 4. The entire spectrum of the hexamer and those of many oligomers in the series have been recorded over a 0–90°C range. The interval between temperature points was 2–4°C in regions where δ changes rapidly with temperature or several protons resonate very close to each other. The interval was ~10°C in temperature regions of little overlap or change in δ. From such data the spectral assignment established at one temperature can be transferred to that at another temperature.

The melding of incremental assignment with an analysis of the temperature effects is needed for the assignment of resonances in the 5–6-ppm region where the nine H_5 and $H_{1'}$ doublets of A_2GCU_2 overlap extensively. For instance, the C(4)H_5 and the $H_{1'}$ signals of A(2), A(1), G(3), and C(4) are well-resolved and can be directly assigned at high temperature for the tetramer and smaller fragments (Figure 3b). However, only the A(2)$H_{1'}$ and G(3)$H_{1'}$ can be unambiguously assigned for the hexamer. The pair of resolved hexamer H_5 resonances can be attributed to C(4) and U(5) and their unique assignments are further discussed below. The other five resonances are enveloped in a broad band at 5.92 ppm, the detailed arrangement of which is not obvious.

The striking spectral changes which occur upon lowering the temperature are illustrated in Figure 3c where the spectra were recorded at 35°C. At this temperature the lines are much better separated and can be correlated to those of Figure 3b by δ vs. T (°C) profiles such as those given in Figures 4 and 5. Many of the δ vs. T (°C) profiles for the molecules with some degree of complementarity (tetramer through hexamer) show dramatic upfield shifts upon decreasing the temperature (Figure 5 and unpublished data). This implies that these molecules begin to self-associate at low temperatures. This causes a spreading of the resonance lines over a wide range as well as crossovers in the δ vs. T (°C) profiles of several of these signals. These crossovers present a further problem in maintaining the identity of an assignment once made, when the crossover takes place with two resonances of the same type of protons with nearly identical coupling constants.

A close examination of Figure 4 shows that the only H_5 resonance crossover occurs at about 75°C for C(4)H_5 and U(5)H_5. These are distinguishable by their unique coupling constants. In fact, the unambiguous assignment for the C(4)H_5 in the hexamer spectra is based on its coupling constant and its δ value as related to those in the tetramer and pentamer spectra. The resonance unambiguously identified as U(5)H_5 in the pentamer spectrum occurs at 5.83 ppm at high temperature (Figure 3b). Upon lengthening the sequence by one pU, the two U-H_5 peaks in the hexamer spectrum appear at 5.85 and 5.90 ppm. (The chemical shift of the latter peak at high temperature is firmly established by tracing its position from the lower temperature data in Figure 4.) The most logical assignments put the U(5)H_5 resonance at 5.85 ppm and U(6)H_5 resonance at 5.90 ppm. The small magnetic anisotropy of the newly added U-base may not substantially increase the δ value of U(5)H_5 but no deshielding is expected. Thus, the reverse assignment would indicate a 0.07-ppm *down*field shift of the U(5)H_5 resonance due to the addition of the U(6) residue, a phenomenon contrary to current understanding. In comparing the tetramer spectra vs. the pentamer spectrum, the most dramatic changes are the resonances from the G(3) and C(4) residues (data to be published). This may be related to the formation of an imperfect duplex involving the middle G·C pairs.

The assignment of the four $H_{1'}$ resonances from the A(1), C(4), U(5), and U(6) residues in the A_2GCU_2 spectrum presents a great challenge; they merge at high temperature (Figure 3b) and they cross each other and with the

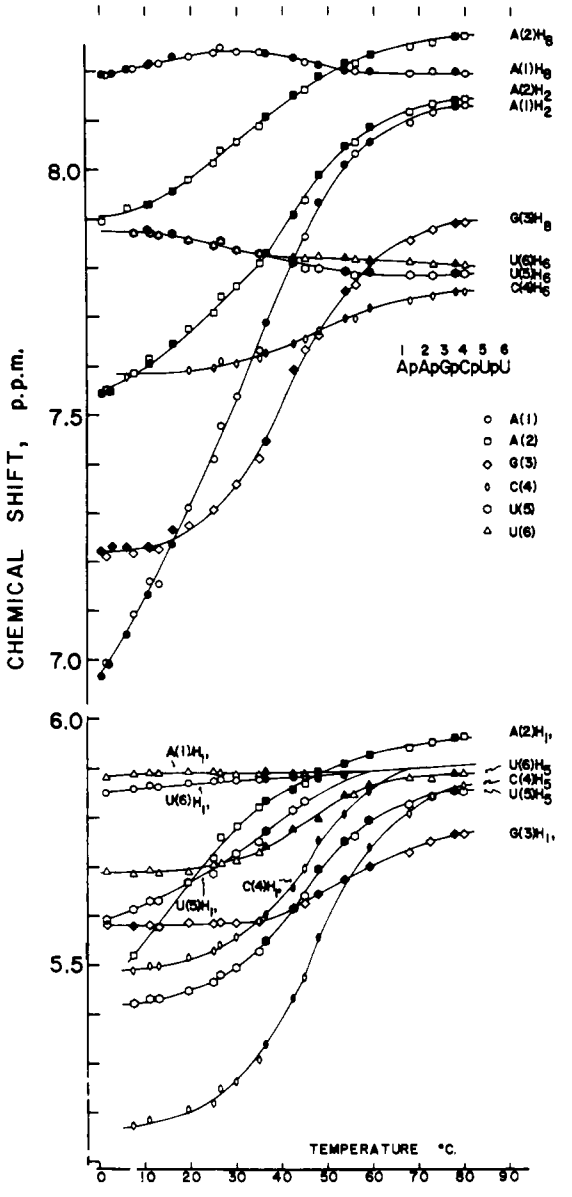

FIGURE 4: The plot of the chemical shifts of base and $H_{1'}$ protons of A_2GCU_2 in D_2O (10 mM in strand concentration, 0.01 M sodium phosphate buffer, pD = 7.0, 0.07 M Na^+) vs. temperature. All chemical shifts are expressed in reference to DSS. The solid symbols represent the data from the 100-MHz spectrometer and the open symbols represent the data from the 220-MHz spectrometer.

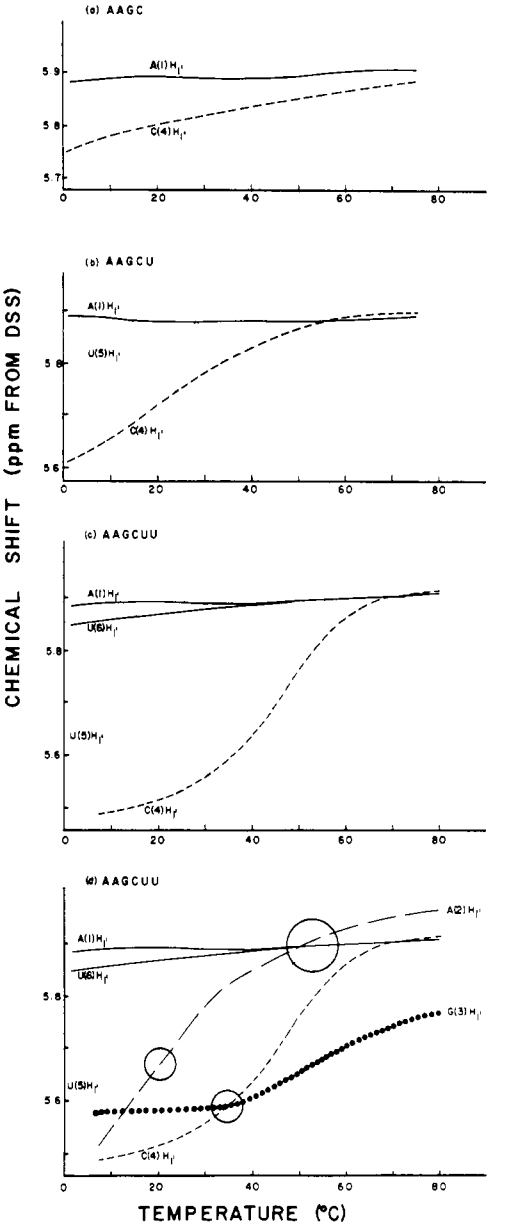

FIGURE 5: The chemical shift (δ) vs. temperature profiles of the $H_{1'}$ resonances. (a) Resonances from the A(1) and C(4) residues in the tetramer A_2GC; (b) resonances from the A(1), C(4), and U(5) residues in the pentamer A_2GCU; (c) resonances from the A(1), C(4), U(5), and U(6) residues in the hexamer A_2GCU_2; (d) all six resonances in the hexamer. Solution conditions are the same as those in Figure 3b and c.

$H_{1'}$ resonances from the G(3) and A(2) residues six times. Figure 5 shows the temperature dependence and tentative assignment of the four remaining $H_{1'}$ signals in the spectra of the tetramer, pentamer, and hexamer. The chemical shift of the resonance appearing in the lowest field is relatively temperature invariant and remains nearly constant in all these oligomers. This resonance can be unambiguously identified as $A(1)H_{1'}$ in AAG and AAGC (Figure 3b and c) and is assigned to the same $H_{1'}$ in the pentamer and hexamer.

The signal of $C(4)H_{1'}$ can be unambiguously identified in the tetramer spectrum as a resonance with a rather large temperature dependence (Figure 5a). In the spectrum of A_2GCU, two $H_{1'}$ resonances are observed upfield from $A(1)H_{1'}$ (Figure 5b). The one with the largest temperature dependence is assigned as $C(4)H_{1'}$ and the other as $U(5)H_{1'}$. The reverse assignment would have to draw the unreasonable conclusion that the addition of the U(5) residue would cause a downfield shift in the $C(4)H_{1'}$ signal. The pentamer spectrum (Figure 5b) shows a relatively large upfield shift for the $C(4)H_{1'}$ resonance. This observation can be explained because C(4) could be strongly stacked upon the neighboring G(3) residue at the initiation site of the A_2GCU helix at low temperatures. The assignment of the other $H_{1'}$ resonance to the U(5) in the A_2GCU spectrum is justified since the U(5) is expected to be less stacked in the imperfect helix. Also, the major shielding of the U(5) residue comes from the neighboring C(4) base which has a ring current magnetic anisotropy smaller than that of G(3) (Giessner-Prettre and Pullman, 1970a). Thus it is reasonable that this $U(5)H_{1'}$ resonance is less temperature dependent than the resonance of $C(4)H_{1'}$.

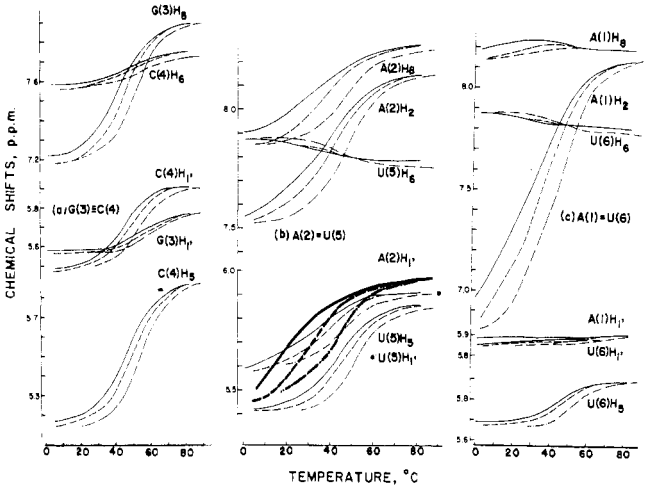

FIGURE 6: The chemical shift vs. temperature profiles of the base and $H_{1'}$ protons of A_2GCU_2 as a function of counterion concentration: 0.07 *M* Na^+ (—), 0.17 *M* Na^+ (- - -), and 1.07 *M* Na^+ (- · · -). The samples were prepared in 0.01 *M* sodium phosphate (pD 7.0), 99.8% D_2O, and were 10 m*M* in strands. (a) The five resonances from the middle G·C pairs, G(3)·C(4); (b) the six resonances from the interior A·U pairs, A(2)·U(5); (c) the six resonances from the terminal A·U pairs, A(1)·U(6). Heavier lines are used in (b) to indicate the $A(2)H_{1'}$ profiles with the same symbols for the various counterion concentrations.

The resonances in the A_2GCU_2 spectrum identified as those from $H_{1'}$ of C(4) and U(5) are both upfield from the signal assigned to $C(4)H_{1'}$ in the pentamer spectrum at all temperatures below ~40°C. Therefore an ambiguity does exist in assignment based only on the low-temperature data. From 40 to 60°C, however, the present assignment allows the $C(4)H_{1'}$ to be more shielded in the hexamer than in the pentamer. The reverse assignment would create an opposite but unacceptable situation. Also, the argument in the preceding paragraph that the shielding effect from a neighboring G is higher than that from a neighboring C supports the assignment shown in Figure 5c, i.e., C(4) is more shielded than U(5) at low temperature. Similarly, the $H_{1'}$ resonances at the lowest field position in the spectrum of A_2GCU_2 have to be assigned to U(6) and A(1), but not to C(4) or U(5) because $C(4)H_{1'}$ and $U(5)H_{1'}$ are expected to be more shielded in the hexamer than in the pentamer. However, the differentiation between the $H_{1'}$ resonances of U(6) and A(1) cannot be made with certainty (Figure 5c). These two resonances have very similar δ values (Figure 5c) and are both from terminal base pairs of the hexamer duplex. The δ vs. *T* (°C) profile of the $H_{1'}$ resonance tentatively assigned to A(1) does conform more closely to the profiles established for $A(1)H_{1'}$ in the tetramer and pentamer (Figure 5a–c).

The simplified δ vs. *T* (°C) profiles were presented in Figure 5c with the implicit assumption that the crossovers of the $H_{1'}$ resonances had been properly resolved. Figure 5d conveys the real problems encountered in analyzing the spectral data. It should be noted that the assignments above the crossover temperatures have been described and established. The problem concerns the portions of the profiles below the crossover. The assignments of the $H_{1'}$ resonances depend upon the third aspect of the assignment procedure: the investigation of ionic strength effects on the δ vs. *T* (°C) profiles. In Figure 6 the solid lines trace the δ vs. *T* (°C) profiles in 0.07 *M* Na^+ and the broken lines indicate the 0.17 *M* Na^+ (- -) and 1.07 *M* Na^+ (- · · -) profiles. The three crossovers which are circled in Figure 5d present the greatest difficulties since these curves intersect with each other at shallow angles. The intersection between 45 and 55°C actually involves a spectral overlap of the four $H_{1'}$ signals from A(1), A(2), U(5), and U(6). The putative $U(6)H_{1'}$ doublet has a larger coupling constant over the entire region than the others so it is rather easily distinguished. The resolution of the multiple crossover at 5.92 ppm depends on the fact that the $U(5)H_{1'}$ resonance splits from this degenerate region at a much higher temperature at higher ionic strengths (Figure 6b). As for the $H_{1'}$ resonances from A(1) and A(2), any attempt to reassign these two $H_{1'}$ resonances after their crossover at 45°C would result in abrupt discontinuities in the two otherwise smooth transition profiles. Thus, the resolution of the crossover of the four δ vs. *T* (°C) curves for these four $H_{1'}$ resonances at 45°C and above can be made with certainty.

The crossover between the $H_{1'}$ resonances of the A(2) and U(5) residues at 20° in Figure 5d presents a considerable problem since the curves could be interpreted as "meeting" instead of "crossing" each other. However, a strong support is gained for the present assignment when the δ vs. *T* (°C) profiles for the two $H_{1'}$ resonances are presented together at three salt concentrations in Figure 6b. Clearly, each family of three curves belonging to one $H_{1'}$ resonance converges at high temperature and segregates at low temperature into nearly parallel lines. These lines have a slope at the midpoint of the transition characteristic of the particular proton. The crossovers occur between the $A(2)H_{1'}$ profiles (heavy lines) and the $U(5)H_{1'}$ profiles (light lines) at ~18°C in 0.07 *M* Na^+, ~32°C in 0.17 *M* Na^+ and ~45°C in 1.07 *M* Na^+ (Figure 6b). The present assignment below the crossover point is dictated by the requirement that the curves in a family be nearly parallel. For instance, the reverse assignment of the 0.17 *M* Na^+ lines below 32°C would destroy the parallelism of the 0.17 *M* Na^+ $A(2)H_{1'}$ with the unequivocally assigned 0.07 *M* Na^+ $A(2)H_{1'}$ curve between 18 and 32°C. Of course, below 18°C the low salt curves are ambiguous and cannot be used in an argument based on parallelism. This argument can be applied in the same way to the $A(2)H_{1'}$ curves in the 32–45°C region, as well as to the $U(5)H_{1'}$ profiles in both regions. It should be noted also, in each of the three salt concentrations, that the two signals merge into a sharp singlet with a line width at half-height about 1.5 Hz in the 220-MHz spectrum recorded at the temperature closest to the crossover point. This very narrow separation (less than 0.01 ppm) of the chemical shifts of these two $H_{1'}$ resonances with their δ vs. *T* (°C) curves meeting at substantially different angles suggests that this crossover is real. If these two curves simply "meet" each other, then an abrupt change of slope is demanded at the point where they meet. The present assignment is also favored by the consideration that the shielding value for $A(2)H_{1'}$ should be larger than that for $U(5)H_{1'}$ since the A(2) residue has two purine neighbors and the U(5) residue has two pyrimidine neighbors.

A similar parallelism argument favors the present assignment of the two $H_{1'}$ resonances of G(3) and C(4) at temperatures below their crossovers (Figure 6a).

Effect of Salt Concentration on Chemical Shifts and the Transition. The chemical shift vs. temperature data can be divided into three groups corresponding to the three unique base-pairing positions in the A_2GCU_2 duplex. Melting curves for the five nonexchangeable protons in each "middle" G(3)·C(4) base pair are shown in Figure 6a at three

Table I: The Chemical Shifts of Formation of 17 Nonexchangeable Protons in (1) the A_2GCU_2 Duplex as Compared with Calculated Ring Current Shifts from Two X-Ray Crystallographic Models and (2) the A_2GCU_2 Coils at 90°C (δ in ppm from DSS).

	Duplex Form						Coil Form	
			$\Delta\delta_{calcd}$[c]		$\Delta\delta_{obsd} - \Delta\delta_{calcd}$			
	δ_{obsd}[a]	$\Delta\delta_{obsd}$[b]	A′	B	A′	B	δ[d]	$\Delta\delta$[e]
$G(3)H_8$	7.20	0.93	0.85	0.33	0.08	0.60	7.91	0.13
$C(4)H_6$	7.56	0.48	0.42	0.21	0.06	0.27	7.77	0.15
$C(4)H_5$	5.14	0.97	1.07	0.66	−0.10	0.31	5.89	0.19
$A(2)H_2$	7.50	0.76	0.64	0.44	0.12	0.32	8.16	0.13
$A(2)H_8$	7.84	0.67	0.79	0.25	−0.12	0.45	8.28	0.27
$U(5)H_6$	7.95	0.07	0.15	0.18	−0.08	−0.11	7.79	0.11
$U(5)H_5$	5.43	0.51	0.46	0.31	0.05	0.20	5.87	0.06
$A(1)H_2$	6.89	1.36	1.05[f]	1.10[f]	0.31[f]	0.26[f]	8.16	0.12
$A(1)H_8$	8.16	0.22	0.00[f]	0.02[f]	0.22[f]	0.20[f]	8.20	0.16
$U(6)H_6$	7.95	0.07	0.03	0.03	0.04	0.04	7.81	0.09
$U(6)H_5$	5.69	0.25	0.20	0.09	0.05	0.16	5.90	0.03
$G(3)H_1'$	5.59	0.35	0.08	0.17	0.27	0.18	5.77	0.13
$C(4)H_1'$	5.48	0.50	0.04	0.07	0.46	0.43	5.92	0.04
$A(2)H_1'$	5.45	0.69	0.10	0.27	0.59	0.42	5.98	0.15
$U(5)H_1'$	5.60	0.38	0.02	0.05	0.36	0.33	5.92	0.08
$A(1)H_1'$	5.86	0.27	0.00	0.22	0.27	0.05	5.92	0.19
$U(6)H_1'$	5.86	0.12	0.00	0.00	0.12	0.12	5.92	0.08

[a] These are the low temperature plateau values of δ at 10 m*M* strand concentration, pD 7.0, 1.07 *M* Na^+. If the 0.17 or 0.07 *M* Na^+ δ vs. *T* (°C) profiles level off at low temperature, their plateau values were averaged with the 1.07 *M* Na^+ number to generate the δ_{duplex} value. [b] $\Delta\delta_{duplex} = \delta_{duplex} - \delta^{0-5°}{}_{mononucleotide}$ is the chemical shift of formation for a proton in the duplex. Appropriate mononucleotide values were selected from the following list (δ in ppm from DSS): pG-H_8, H_1', 8.126, 5.936, respectively; pC-H_6, H_5, H_1', 8.038, 6.110, 5.979; pA-H_2, H_8, H_1', 8.257, 8.512, 6.141; pU-H_6, H_5, H_1', 8.015, 5.935, 5.982; and Ap-H_2, H_8, H_1', 8.252, 8.381, 6.132, measured in 0.01 *M* sodium cacodylate buffer, pD 5.9 ± 0.1 in D_2O, 1 m*M* in the appropriate 5′-mononucleotide (a 2.0 m*M* sample of 3′-AMP was also measured). Little or no association of the mononucleotides is expected at these low concentrations. Temperatures were 0–5°C. [c] Based on the A′-RNA and B-DNA geometries (Arnott et al., 1972; Arnott and Hukins, 1972) and ring current isoshielding contours provided by B. Pullman (private communication, see Discussion). [d] These averages of the 90°C chemical shifts of protons in 0.07, 0.17, and 1.07 *M* Na^+ at 10 m*M* strand concentration, pD 7.0. [e] $\Delta\delta_{coil} = \delta_{coil} - \delta^{90°}{}_{mononucleotide}$ is the chemical shift of formation for a proton in the high temperature coil form. These mononucleotide values were used (see note b for buffer and nucleotide concentrations): pG-H_8, H_1', 8.041, 5.890; pC-H_6, H_5, H_1', 7.921, 6.084, 5.960; pA-H_2, H_8, H_1', 8.287, 8.547, 6.130; pU-H_6, H_5, H_1', 7.905, 5.930, 6.001; and Ap-H_2, H_8, H_1', 8.282, 8.359, 6.109. [f] These calculated values are subject to a correction of ~0.15 ppm due to shielding in end-to-end aggregates.

salt concentrations. Likewise, the curves for the six protons in each "interior" A(2)·U(5) pair appear in Figure 6b, and the six protons in each "terminal" A(1)·U(6) pair in Figure 6c. Each of the curves was generated from 10 to 20 spectra covering the entire temperature range.

For a given resonance, the overall shape of the curve remains nearly the same for all three salt concentrations. At 90°C, the three curves for each proton approach the same limiting δ value. The resonances in appropriate fragments and hexamer spectra at 1 m*M* in strands and 0.02 *M* Na^+ also show the same properties at high temperature (unpublished results). This implies that these oligonucleotides have the same average single-strand conformation at high temperature over this range of salt and strand concentration. The average values at 90°C are indicated in Table I and represent the chemical shifts of the resonances in the single-strand coil. At low temperature these curves appear to level off at a constant limiting value. This tendency is particularly evident in the curves for the highest salt concentration and in the data for the G(3)·C(4) pair (Figure 6a) and the A(2)·U(5) pair (Figure 6b). An extrapolated value of this limiting chemical shift at low temperature is taken to represent the chemical shift of the resonance in the helical duplex; these values are listed in Table I.

The data in Figure 6 also illustrate the dramatic changes in chemical shifts of these resonances over this temperature range. Some are shifted by about 1 ppm. Upon decreasing the temperature, 12 resonances show cooperative transitions in upfield shifts. Most of these changes greatly exceed the temperature effects observed with unassociated oligo- and mononucleotides which are usually less than 0.2 ppm. For the 12 resonances which show a sizable upfield shift on helix formation, the temperatures (T_m) at the maximal slope of the melting curves increase at higher salt concentrations (Table II). Also, the nature of the low-temperature portions of the transition curves becomes more evident with increasing salt concentration. There are five protons, $A(1)H_8$, $U(5)H_6$, $U(6)H_1'$, $A(1)H_1'$, and $U(5)H_6$, whose resonances change little or even move downfield upon decreasing the temperature. $A(1)H_8$ exhibited a small downfield shift at intermediate temperatures, a shift which became smaller at higher salt concentrations. The U(5) and $U(6)H_6$ resonances at low temperature showed a small downfield shift which became *larger* at higher salt concentration. The $A(1)H_1'$ and $U(6)H_1'$ resonances shifted very slightly upfield on decreasing the temperature, and this shift became larger on increasing the salt concentration. All these changes in resonance position are relatively minor compared to those observed for other resonances.

A final note of importance for this section is that the sample in 1.07 *M* Na^+ became cloudy on lowering the temperature to 30°C. The turbidity increased considerably at lower temperatures. This precipitation was not observed at other salt concentrations.

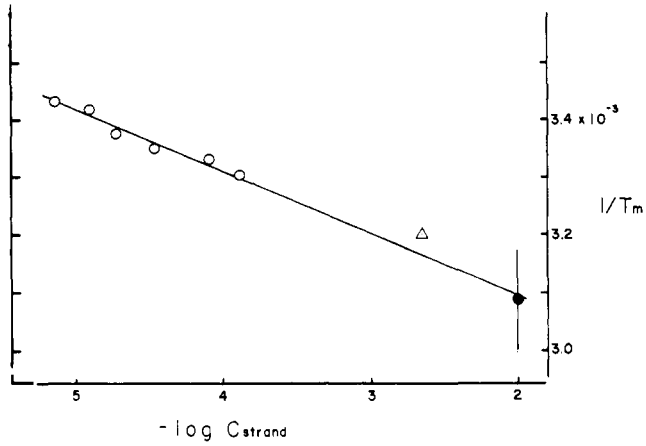

FIGURE 7: The $1/T_m$ vs. log C_{strand} plot constructed from uv absorbance melting data at low (○) and high (△) strand concentration as well as from an average of the ^1H NMR transition temperatures (●); the range of T_m values for the individual protons in the ^1H NMR experiments is represented by the vertical bar. The samples contained 0.99 *M* NaCl, 0.01 *M* phosphate buffer (pH 7.0) (or pD 7.0 in the ^1H NMR experiments), and 10^{-4} *M* EDTA. The uv absorbance melting data at low concentration (○) is from Borer et al. (1974).

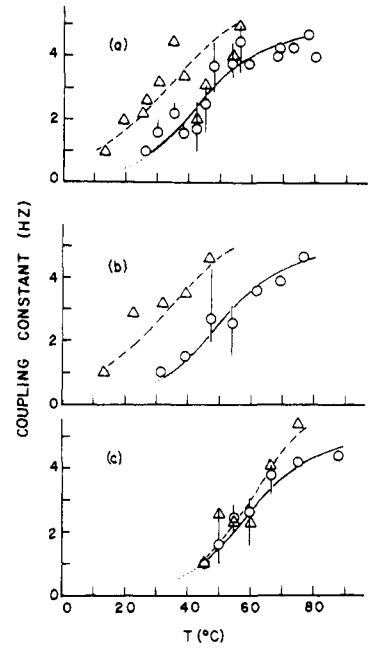

FIGURE 8: The $H'_{1'}$-$H_{2'}$ coupling constants, $J_{1'-2'}$, for the six ribose $H_{1'}$ resonances of A_2GCU_2 as a function of temperature and counterion concentration: (a) 0.07 *M* Na^+, (b) 0.17 *M* Na^+, (c) 1.07 *M* Na^+. The $J_{1'-2'}$ values for the tentatively identified U(6)$H_{1'}$ signal (- - -) were plotted separately from the average of the other five resonances (—). The vertical bars indicate the range of values observed for these five signals and the lowest temperature point indicates the temperature at which all the resonances become singlets with $J_{1'-2'} \leq 1.5$ Hz.

Circular Dichroism (CD) and Ultraviolet Absorption Studies on the Helix-Coil Transition. The CD and uv absorption of a sample of A_2GCU_2 at 2.22 m*M* strand concentration (13 m*M* in residue concentration), 1.03 *M* Na^+, 0.01 *M* PO_4^{3-} (pH 7.0), and 10^{-4} *M* EDTA were studied in ultrathin optical cells. No turbidity in this sample was detected at 0°C. Within experimental error, the CD spectrum of this sample measured at 0°C is identical with the published spectrum of A_2GCU_2 measured at 8.9 m*M* residue concentration, 0°C, in 1 *M* NaCl (Borer et al., 1973). The CD results on this A_2GCU_2 sample, newly prepared in our laboratory, confirm the identity and the CD data of the A_2GCU_2 prepared previously.

The maximal slope of the transition in the A_{260} vs. *T* (°C) profile of this A_2GCU_2 sample was found at 40 ± 5°C. As shown in Figure 7, this value is about 3° lower than that predicted in a $1/T_m$ vs. log strand concentration plot based on previous uv studies at lower concentrations (Borer et al., 1974b). This $1/T_m$ vs. log *C* plot (Figure 7) also shows the correspondence between the T_m values (open symbols) obtained from uv measurements at lower strand concentrations and the averaged T_m value obtained from the ^1H NMR melting curves (Figure 6). The satisfactory agreement between the T_m values obtained by these two different techniques over a 10^3-fold concentration range is indeed noteworthy.

The hypochromicity in the absorbance vs. temperature profiles was found unexpectedly to be concentration dependent. (The % hypochromicity = $100(A_{50} - A_0)/A_{50}$, where A_{50} is the absorbance of the single strand at 50°C and A_0 is the absorbance of the helical duplex at 0°.) The hypochromicity in 1 *M* NaCl was 16–18% between 7 and 130 μM strand concentration for six measurements. The measurement of the present sample at 2.2 m*M* was 23–25%. The relatively large uncertainty (±5°C) of the T_m reported above is due to this phenomenon. In addition, the absorbance appeared to decrease further below 0°C instead of leveling off. Preliminary experiments on a sample of 10 m*M* strand concentration in 0.17 *M* Na^+ indicated a hypochromicity of 26–29%. The large values of hypochromicity and its concentration dependence, the continuing decrease of absorbance at low temperature, and the precipitation observed at low temperatures in high salt and oligonucleotide concentrations are indications that multimolecular aggregation among the helical duplexes can take place under certain conditions.

Temperature and Ionic Strength Dependence of the Ribose $H_{1'-2'}$ Coupling Constants. The accuracy of the coupling constant measurements in these ^1H NMR spectra is estimated to be ±1 Hz. This estimation comes from the ±0.5 Hz uncertainty in the spectral position of a resonance in a 220-MHz spectrum recorded in the Fourier transform mode with a 4 K data table and a bandwidth of 2000 Hz. (The 100-MHz spectra were recorded with a 4 K data table and a 1000-Hz bandwidth.) This causes the measurements of the individual $J_{1'-2'}$ values to be scattered considerably. Furthermore, the $H_{1'}$, H_5 resonances cross and overlap extensively throughout the entire temperature range, and at low temperatures the signals broaden and are crowded by the downfield shift of the large HOD peak. Nevertheless, much valuable information can be gained from the general trend of the effect of temperature on the $J_{1'-2'}$ values. Figure 8 illustrates the properties of the average (circle symbols) and range (vertical bar) of the $J_{1'-2'}$ values of the five $H_{1'}$ doublets which decrease most rapidly upon decreasing the temperature. The $J_{1'-2'}$ values for the tentatively assigned U(6)$H_{1'}$ resonance (triangle symbols) are plotted separately. At high temperatures the $J_{1'-2'}$ values are close to those observed for the appropriate nucleoside monophosphates (e.g., see Ts'o, 1970). Upon decreasing the temperature these doublets become narrow with smaller *J* values; they merge into a singlet within the resolution of the spectrometer at a sufficiently low temperature. Therefore, the $J_{1'-2'}$ values are less than 1.5 Hz for the furanose ring of each residue in the helical duplex. The temperatures at

which all of the $H_{1'}$ resonances appear as singlets are shown in Figure 8. Although the shapes of the $J_{1'-2'}$ vs. T (°C) profiles in Figure 8 are not well defined because of the scattered measurements, the positive influence of ionic strength on the transition temperature is clearly demonstrated. This positive influence of the ionic strength on the $J_{1'-2'}$ vs. T (°C) profiles can be correlated with the same influence on the δ vs. T (°C) profiles (Figure 6). Such a correlation unambiguously establishes that the thermally induced transitions in the coupling constants of all the residues reflect the helix–coil transition of the A_2GCU_2 duplex.

Further clarification of the trends in the individual J values during the transition may be made by comparing the resonances at intermediate temperature where the helix is partially melted. The coupling constants typically have the order: $C(4) \simeq G(3) \simeq A(1) < A(2) \simeq U(5) \ll U(6)$.

It should be noted that $J_{1'-2'}$ values of the purine mononucleotides (~6 Hz) are slightly larger than those of the pyrimidine mononucleotides (~4 Hz); also that the assignments for the A(1) and U(6)$H_{1'}$ are tentative and will be justified later. A further investigation on the properties of the individual $H_{1'}$ resonances during the helix–coil transition is currently in progress on a higher frequency spectrometer with greater resolution and accuracy.

Discussion

The Assignment Procedure. The general applicability of the powerful procedure which combines incremental assignment with careful analyses of the effects of systematic temperature and ionic strength variations is well demonstrated in the unambiguous, albeit indirect, assignment of 15 of the 17 bases and ribose $H_{1'}$ resonances of A_2GCU_2. These assignments can be regarded with confidence because of three factors. (1) Each residue that is added to a single-stranded oligonucleotide must exert a shielding effect primarily on the protons of its nearest neighboring residue on the preexisting segment. This phenomenon is inevitably observed and is confirmed in cases where the assignments are known. This basic principle of the incremental assignment approach is applicable particularly when the newly added residue carries an aromatic base which, even in single-stranded oligomers, has a tendency to take part in the parallel stacking of bases. (2) Each δ vs. T (°C) profile is continuous with no abrupt changes of slope. Thus, a spectral assignment can be transferred from a spectrum at one temperature to another provided a sufficient number of spectra are taken to establish the correct shape of the profile. The continuity and shape of the profiles are determined by the changes in local magnetic environment induced by the structural transition. (3) Each of the δ vs. T (°C) profiles for a proton are parallel at the three ionic strengths reported. The near identity in the shape of these profiles implies that the thermally induced structural transition occurs in a similar fashion at each ionic strength. The parallelism of the δ vs. T (°C) profiles provides a firm basis for resolving crossovers of resonances.

Geometrical Constraints Imposed on the A_2GCU_2 Helix by the Coupling Constants, $J_{1'-2'}$. An accurate description of the geometry of the A_2GCU_2 double helix *in solution* is obviously the major goal of this investigation. The importance of this goal rests on the assumption that the geometry of the short helix will be nearly identical with the geometry of the helices found in natural RNA. The validity of the assumption and the attainment of the goal are based on a careful comparison of the ^1H NMR results on the short helix in solution with X-ray diffraction results on long helical nucleic acids in the fiber form.

Results from X-ray diffraction studies and from model building firmly establish the furanose conformation as a major parameter in the characterization of double helix geometry. In general, the furanose ring pucker falls into one of four conformers (e.g., see Ts'o, 1974a) for which $J_{1'-2'}$ values have been computed (Smith and Jardetzky, 1968). The conformers are named according to the ring atom farthest from the $C_{4'}$–O–$C_{1'}$ plane and whether the atom is on the same side of the ring as the $C_{5'}$ atom (endo) or on the opposite side (exo). Brackets indicate the pairs of conformers (with their calculated $J_{1'-2'}$ values) which are physically very similar to each other: [$C_{3'}$-endo (0.4 Hz), $C_{2'}$-exo (0.2 Hz)] and [$C_{2'}$-endo (8.6 Hz), $C_{3'}$-exo (4.6 Hz)].

In a series of papers, Arnott, Hukins, and their coworkers reported the refinement of the geometry of nucleic acid helices based on X-ray fiber diffraction patterns. A special emphasis was placed on the furanose conformation. For example, Arnott and Hukins (1972) stated that, "The major difference between A- and B-DNA is in the conformation of the furanose ring that is $C_{3'}$-endo for A and $C_{3'}$-exo for B." In a previous paper in 1969, Arnott et al. first proposed a $C_{2'}$-endo conformation for B-DNA, but their later analysis (Arnott and Hukins, 1973) encouraged them to specify the $C_{3'}$-exo form. Similar studies on RNA helices led them to definitely recommend $C_{3'}$-endo for the A- and A′-RNA forms, which are very similar to the A-DNA structure (Arnott et al., 1972, 1973). Analyses of high-resolution diffraction patterns of crystalline rApU (Rosenberg et al., 1973) and rGpC (Day et al., 1973) have also been reported. Both of these self-complementary dinucleoside phosphates crystallize into forms very similar to A-RNA with the $C_{3'}$-endo furanose conformation.

In general, the $J_{1'-2'}$ data on the nucleosides and nucleoside 5′-monophosphates indicate that their furanose conformation in aqueous solution is not frozen in a given conformation but exists in a dynamic equilibrium among several forms. Most of the coupling constant data, such as those of $J_{1'-2'}$, have been analyzed previously in terms of populations of the $C_{2'}$-endo and $C_{3'}$-endo forms since they were the most commonly observed crystal forms; also the $J_{1'-2'}$ data cannot be justifiably analyzed with more than two unknown parameters.

The results from the present investigation clearly establish that the $J_{1'-2'}$ of each residue in the A_2GCU_2 duplex is less than 1.5 Hz. Therefore, the equilibrium distribution of furanose conformations in this short ribosyl helix must have very small populations of the $C_{2'}$-endo and $C_{3'}$-exo forms. The $J_{1'-2'}$ values indicate either the $C_{3'}$-endo or $C_{2'}$-exo as the predominant conformation. Their physical similarity makes an absolute distinction unnecessary, but in view of the rarity of the $C_{2'}$-exo form in the crystal studies it is most logical to consider that the furanose in this short helix is principally in the $C_{3'}$-endo form. Thus, the $H_{1'}$–$H_{2'}$ coupling constants in the A_2GCU_2 helix provide direct verification that RNA double helices in solution have a conformation similar to that observed by X-ray diffraction in fibers and crystals. A choice of one of the "A-type" conformations is clearly favored over the "B-type" arrangement.

A general characteristic of single-stranded oligo- and polynucleotides containing only purines is that their $J_{1'-2'}$ values decrease rapidly with temperature from 5 to 6 Hz above 70°C to 1–2 Hz at low temperatures (Hruska and Danyluk, 1968; Ts'o et al., 1969; Alderfer and Smith, 1971;

Table II: T_m (°C) of 12 Chemical Shift vs. Temperature Profiles Observed in the A_2GCU_2 Helix to Coil Transition: Dependence on NaCl Concentration.[a,b]

	Salt Concentration		
	1.07 *M*	0.17 *M*	0.07 *M*
$G(3)H_8$	51	45	42
$C(4)H_6$	60	55	48
$C(4)H_5$	55	52	48
$G(3)H_{1'}$	62	59	55
$C(4)H_{1'}$	55	50	47
$A(2)H_2$	45	41	37
$A(2)H_8$	47	38	34
$U(5)H_5$	52	49	45
$A(2)H_{1'}$	46	35	25
$U(5)H_{1'}$	49	43	40
$A(1)H_2$	42	35	31
$U(6)H_5$	52	50	45

[a] The T_m is defined as the temperature of maximum slope of a δ vs. T (°C) profile. [b] The strand concentration is 10 m*M* and pD 7.0.

Kondo et al., 1972; J. L. Alderfer and P. O. P. Ts'o, unpublished results). On the contrary, Kreishman and Chan (1971) found that the $J_{1'-2'}$ value for poly(U) was temperature independent. The purine polynucleotides are stacked to a much greater extent at low temperatures so the difference in the two types of polymers could be due to the small tendency of uracil bases to stack or the absence of steric interference from the 2'-OH to the stacking form of pyrimidine polynucleotides. This difference does, however, provide a justification for assigning the A(1) and $U(6)H_{1'}$ resonances in the A_2GCU_2 spectra. It was noted that the putative $U(6)H_{1'}$ signal had a substantially larger coupling constant than the other resonances (see Figure 8). Current hypotheses indicate that helix melting proceeds from the ends toward the middle and that the end base pairs have a considerably lower stability than the others. This hypothesis is supported by the NMR data in Table II and in the accompanying paper (Kan et al., 1975a). Thus, the average conformations of the terminal bases should be more like the single strands than any of the interior bases. It has already been indicated that the RNA double helix geometry strongly favors the $C_{3'}$-endo form so the interior bases should have generally smaller coupling constants. The furanose moiety of the A(1) residue should favor the $C_{3'}$-endo form even at temperatures where the population of paired A(1) residues is relatively small because of its tendency to stack on A(2); whereas at this temperature the furanose of U(6) should still be in a dynamic equilibrium with substantial populations of conformers having large $J_{1'-2'}$ values. It is also noteworthy that U(6) is the 3'-OH terminal residue so its furanose ring would not be expected to encounter a push from the 2'-OH group to the $C_{3'}$-endo form upon stacking. It should be noted that the U(6) furanose does assume the $C_{3'}$-endo form at low enough temperatures, so the energetics of sugar conformational changes in the coil–helix transition must involve effects from the helical structure other than 2'-OH steric interference.

Geometrical Constraints Imposed on the A_2GCU_2 Helix by the Chemical Shifts of Formation of the Duplex ($\Delta\delta_{duplex}$). Additional information about the geometry of the A_2GCU_2 helix in solution comes from the data on chemical shifts. As described in Results, the limiting values of the chemical shifts at low temperature for each resonance were averaged for the three salt concentrations. These "δ_{duplex}" values are taken to represent the chemical shifts of the resonances in the helical duplex. Similarly, the averaged values at 90°C, "δ_{coil}", are taken to represent the chemical shifts of the resonances in the coil state (see Table I). The chemical shift of formation of the duplex is defined as: $\Delta\delta_{duplex} = \delta_{duplex} - \delta^{0-5°}{}_{mononucleotide}$, where the chemical shift of the same proton in an appropriate mononucleotide at nearly infinite dilution is the reference state. (The measured chemical shifts carried a negative sign in the original convention, which is now usually omitted; thus, increased shielding is reflected in a positive chemical shift of formation.) In the same vein, the chemical shift of formation of the coils at high temperature is defined as: $\Delta\delta_{coil} = \delta_{coil} - \delta^{90°}{}_{mononucleotide}$. $\Delta\delta_{duplex}$ and $\Delta\delta_{coil}$ are directly analogous to the dimerization shifts $\Delta\delta_D{}^{t°}$ and polymerization shifts $\Delta\delta_P{}^{t°}$ employed extensively by NMR spectroscopists examining the conformation of dinucleotides and polynucleotides (e.g., see Ts'o, 1974b; Alderfer et al., 1974). Their values approximate the through-space diamagnetic and paramagnetic changes in the local field experienced by the proton in question. The $\Delta\delta$ values represent the differential shielding encountered in the process of bringing together isolated nucleotides, forming the covalent phosphodiester links, and allowing the associated residues to assume the conformation under investigation. Implicit in the above approach is the assumption that any through-bond effects are localized to the nuclei near the newly formed phosphodiester bond. To further reduce these effects the chemical shift of the monoanion of the nucleoside 5'-monophosphate, studied at pD 5.9, is used for the reference state. The only known effect diester formation has on the base and $H_{1'}$ protons in single-stranded nucleic acids is an ~0.05-ppm shielding increase for the purine H_8 and pyrimidine H_6 protons of diesterified residues as compared to the singly ionized nucleoside 5'-monophosphate (Ts'o, 1974b).

Most of the chemical shifts of formation observed in single-stranded di-, oligo-, and polynucleotides apparently originate from the shielding effect of the ring-current magnetic anisotropy of the neighboring bases (Ts'o, 1974a,b). This is also probably true for $\Delta\delta_{duplex}$ values. If the origins and magnitudes of the local magnetic fields together with their distance dependence were known, the spatial relationships of the various protons and magnetic centers could be established from the $\Delta\delta_{duplex}$ values. In principle, then, the 17 C–H and 3 N–H $\Delta\delta_{duplex}$ values define the geometry of the A_2GCU_2 helix. The accuracy and completeness of the definition of the geometry depend on (1) the accuracy of the $\Delta\delta_{duplex}$ measurements; (2) a detailed description of the local magnetic centers and their field effects; and (3) the number and locations of the protons (or other atoms) which can be studied by NMR. At the current level of development of the art and science of NMR, an atomic model of the A_2GCU_2 helix in solution cannot be constructed solely from the chemical shift data. As shown in the succeeding paragraphs, the $\Delta\delta_{duplex}$ values are useful for making a critical choice between two helical models constructed from the X-ray diffraction data on fibers.

A complete helical model of A_2GCU_2 was constructed from the coordinates of A'-RNA given by Arnott, Hukins, and coworkers (Arnott and Hukins, 1972; Arnott et al., 1973). The geometry of A-RNA (11 bases per helical turn) and that of A'-RNA (12 bases per turn) are close enough to each other to be indistinguishable by NMR. A'-RNA is the form observed when the fibers are drawn from solutions of high ionic strength, so it was chosen for comparison with

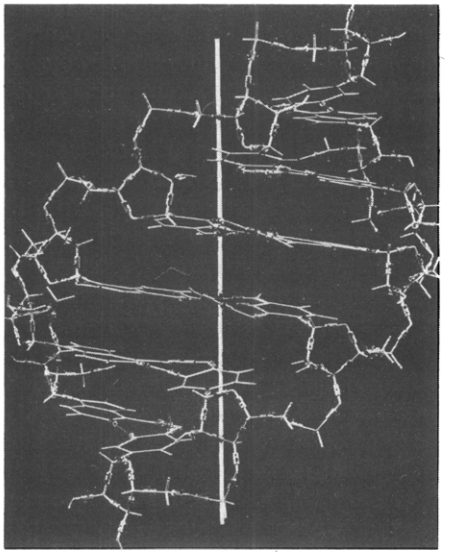

FIGURE 9: A view of the Kendrew model of the A_2GCU_2 duplex built in the A′-RNA geometry according to the coordinates of Arnott et al. (1972). The view is approximately along the dyad axis of the G(3)·C(4) pair, which is the third base pair from the bottom and faces the minor (or shallow) groove of the helix with the helix axis indicated behind the base pairs. The photograph introduces a slight parallax distortion into the spatial relationships of the atoms; however, the approximate scale may be deduced from the axial rise per residue of 3.00 Å for A′-RNA.

the ^1H NMR data since the duplex is most stable at high salt concentrations. The principal difference in the two models is the smaller "tilt" of the bases in the A′-RNA model.

A photograph of the A_2GCU_2 helix built with Kendrew molecular models is shown in Figure 9, which is a view into the "shallow" or minor groove. The view is approximately along the dyad axis of the G(3)·C(4) pair which is the third pair from the bottom, and is perpendicular to the helix axis which is shown behind the bases. The near parallelism of the furanose rings with the helix axis is apparent in the middle two base pairs; the base pairs are tilted with respect to the helix axis by about 10° and the bases have a propeller-like "twist" of about 8°. The projections of neighboring protons onto the plane of each base were made from the Kendrew model and are shown in Figure 10. The distances along a normal to the base planes are indicated in parentheses, as well as the projections and distances of protons within the shielding region of next-nearest neighboring bases. The three-dimensional model shown in Figure 9 and the projections shown in Figure 10 provide the geometrical basis for comparing the $\Delta\delta_{duplex}$ data with the A′-RNA fiber form.

An incomplete model of the A_2GCU_2 helix was also constructed from the coordinates of B-DNA recommended by Arnott and Hukins (1973). Projections of the neighboring protons onto the plane of each base in the hexamer were also made, similar to those displayed in Figure 10. The model and the projections provided the necessary information for the computation of the predicted $\Delta\delta_{duplex}$ values based on the B-DNA geometry.

The predicted chemical shifts of formation for the A_2GCU_2 sequence in both the A′-RNA and B-DNA geometries are reported in Table I. The computation used ring current isoshielding contours mapped in planes parallel to the bases at the distances shown in Figure 10. These contours were generously provided by Dr. B. Pullman (private communication) and were calculated by the procedure given by Giessner-Prettre and Pullman (1970a). Such calculations accurately account for the distance effects intro-

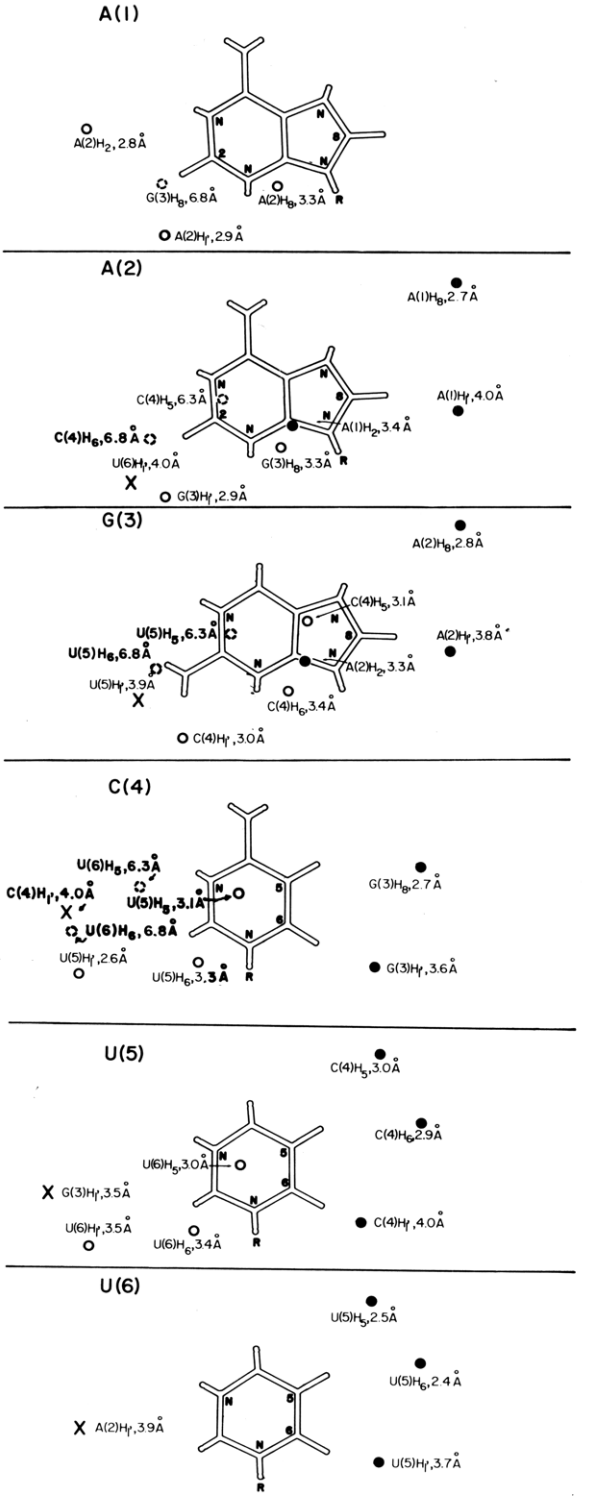

FIGURE 10: The projections of neighboring protons onto the plane of each base of the A_2GCU_2 helix (A′-RNA geometry). Projections and distances were taken directly from the Kendrew model shown in Figure 9. (O) Protons positioned below the base plane; (●) protons positioned above the plane; (O) protons from a distant neighbor about 6.8 Å away; and (×) $H_{1'}$ atoms in the other strand. The views are normal to the base planes with the free 5′-OH terminus above and the 3′-terminus below the base planes. Vertical distances of the protons to the base planes are indicated in parentheses.

duced by the twisting and tilting of bases in the RNA helix as well as next-nearest neighbor effects. In regard to the latter, it is interesting to note that adenine is calculated to exert a maximum shielding of 0.20 ppm at a 6.8-Å vertical distance. In the 6.8-Å plane, the effect falls off much more gradually with the horizontal distance from the ring than for contours in the 3.4-Å plane. For instance, the vertical projection of G(3)H_8 on the A(1) plane is about 4 Å away from the point of maximum shielding (Figure 10), yet the calculated shielding of 0.10 ppm reaches half the maximal value. The distant neighbor isoshielding contours predict the following values (in ppm; see Figure 10 for distances): G(3)H_8, 0.10 from A(1); C(4)H_6, 0.10 from A(2); C(4)H_5, 0.20 from A(2); U(5)H_6, 0.04 from G(3); U(5)H_5, 0.11 from G(3); and U(6)H_5, 0.03 from C(4).

In comparing the predicted and observed chemical shifts of formation it is important to set reasonable error limits for the calculations. A major source of uncertainty in the predictions is that the isoshielding contours are generated by an approximate molecular orbital calculation. Thus, agreement between the calculations and predictions within 0.1 ppm is probably as good as can be expected. It should also be noted that the original calculations of this type (Waugh and Fessenden, 1957; Johnson and Bovey, 1958) dealt with benzene. Such a treatment may be more hazardous for some of the nucleic acid bases which have more localized π electrons. An examination of Table I shows that the calculated $\Delta\delta_{duplex}$ values for 9 of the 11 base protons agree to within 0.12 ppm of the observed values. The other two calculations are still qualitatively correct; a very large shift is predicted for A(1)H_2 and a small shift for A(1)H_8. On the contrary, only 2 of the 11 predictions from the B-DNA model are correct within 0.12 ppm. Thus, a base stacking geometry similar to that in the A'-RNA model is clearly favored over the B-DNA conformation according to this analysis.

It is useful to discuss the remaining serious discrepancies in the chemical shift data, and to point out magnetically anisotropic effects from sources other than the heterocyclic rings as well as the influence of minor deviations from standard RNA conformation. These effects are apparently much smaller in magnitude than the ring current effects for the base protons, but must exert a substantial influence on the $\Delta\delta_{duplex}$ values of the $H_{1'}$ (Table I, bottom). It is hoped that the following detailed discussion of these effects may stimulate future attempts to investigate this important problem.

(*1*) *Effect of Multiple Aggregation.* It was noted in Results that evidence from hypochromicity, resonance line widths, and a sample turbidity suggested the existence of some form of multiple aggregation of the duplexed strands. The association of mononucleosides and -tides in water has been studied extensively by NMR and thermodynamic methods (for review see Ts'o, 1974a). Association persists even at the level of 10 m*M* AMP, as followed by the concentration dependence of the base and sugar proton resonances. The concentration of end A(1) bases in duplexed A_2GCU_2 was 10 m*M* in the studies presented here. Therefore, it is not unreasonable that several duplexes might form an end-to-end stacking arrangement similar to that seen for the mononucleotides. This notion is supported by studies with intercalative agents that disrupt this type of association (Kan et al., 1975b). These experiments suggest that this effect may account for 0.1–0.15 ppm of the observed $\Delta\delta_{duplex}$ for A(1)H_2 and A(1)H_8. This additional shielding increment brings the calculated $\Delta\delta_{duplex}$ values for these A(1) protons within about 0.15 ppm of those observed. Thus the agreement between the calculated and observed chemical shifts of formation for the base protons is remarkable if this correction based on aggregation is applicable.

(*2*) *Cross-Strand Deshielding Effects.* Protons located approximately in the plane of an aromatic ring encounter a ring current effect which causes them to resonate at lower field. This deshielding must be quite small for the nonexchangeable protons in base pairs because of the large horizontal distances involved. The greatest effect might be expected from adenine upon the H_5 and H_6 of uracil in the A·U pair. However, these protons are about 8 Å removed from the center of the six-membered ring of adenine. It is not likely these protons will be deshielded by more than ~0.1 ppm. This effect (or combined with effect (4) below) may be the origin of the inverted δ vs. T profiles for the U-H_6 protons seen in Figure 6b and c.

(*3*) *Solvent Exclusion Effects.* This consideration primarily concerns the effect of excluding the solvent from the rather acidic H_8 protons. Katz and Penman (1966), Hruska et al. (1968), and Ts'o et al. (1969) experimented on the effect of transferring various purine bases from aqueous solution to Me_2SO, and found a degree of hydrogen bonding of the solvent to the H_8 proton. The H_8 protons are effectively transferred to a hydrophobic environment upon the formation of the A_2GCU_2 duplex. Therefore, these protons are expected to be more shielded in the duplex than in the mononucleotides. The Me_2SO to D_2O transfer experiments suggest an upper limit of 0.1–0.15 ppm for this effect and no effect on H_2 and $H_{1'}$ protons. This effect is probably smaller for the terminal, A(1)H_8 proton.

(*4*) *Base–Base Hydrogen Bonding.* The electronic nature of the bases is changed by hydrogen bonding. The principal effect will be on the adenine and cytosine bases due to the formation of NH–N hydrogen bonds at adenine N_1 and cytosine N_3. Hydrogen bonds at other loci on the four bases involve exocyclic bonds and will therefore have little influence on the π-electron system of the bases. The situation is somewhat analogous to ring protonation and this analogy may be used to estimate the direction of the hydrogen bonding effects and their upper limits; 1 m*M* solutions of adenosine and cytidine in D_2O were acidified with DCl to their pk_{a_1} values. These values closely correspond to the D^+ concentration necessary to produce 50% ionization of the bases. The changes in measured chemical shifts (referred to the δ values at pD $\simeq$ 7) were doubled to give these chemical shifts of ionization: A-H_2 = 0.22, H_8 = 0.24, $H_{1'}$ = 0.10; and C-H_6 = 0.28, H_5 = 0.16, $H_{1'}$ = −0.01. All values are given in ppm and represent downfield shifts relative to the nonionized form. However, it is expected that they are a considerable overestimate of hydrogen bonding effects. The presence of a formal positive charge should decrease electron density and deshield the ring protons more than a hydrogen bonding proton. Also the nonionized reference state must have considerable hydrogen bonding to water, so the change from one hydrogen bonded state to another should not induce a very large change in electron density.

The direct observation of base pairing of mononucleosides or free bases has proved impossible in aqueous solution due to the low stability of such complexes and the tendency of the bases to self-associate. However, several reports have presented chemical shift data on protons of such base pairs in organic solvents. Newmark and Cantor (1968), Katz and Penman (1966), and Shoup et al. (1966) studied G·C pair-

ing in Me_2SO and Me_2SO–dimethylformamide mixtures, Katz (1969) studied A·U pairing in $CHCl_3$, and Giessner-Prettre and Pullman (1970b) calculated the combined effects of cross-strand ring currents and the inductive effect of pairing in these studies. However, these data cannot be directly compared with the situation in water due to differences in hydrogen bonding of solvent to the bases in the unpaired, reference state. Also, even in organic solvents, it is difficult to analyze the data to obtain chemical shifts characterizing the totally Watson–Crick paired species.

The data on protonation and base paired monomers lead to a maximum deshielding of ~0.1 ppm for the A and C base protons with negligible effects on the base protons of G and U, and all $H_{1'}$ protons.

(*5*) *Effect of the Change of Furanose Conformation.* The ring oxygen atom, $O_{1'}$, has a magnetic anisotropy associated with its two sets of lone-pair electrons. The change of furanose conformation should have a larger effect on the $H_{1'}$ resonances than on the others. The ribose rings in $(A_2GCU_2)_2$ favor the $C_{3'}$-endo conformation in the helix as described above. However, the reference state for the shielding calculations is the mononucleotide which has been shown to have its furanose ring in a dynamic equilibrium among several states. Thus, some of the differential shielding observed for $H_{1'}$ may be attributable to a difference in the average positions of these protons with respect to O-1′. In an attempt to characterize this effect, the $H_{1'}$ resonance of adenosine 3′,5′-cyclic phosphate (<pA) was compared with that of the pA and Ap monoanions. Smith and Jardetzky (1968) defined the furanose conformation of <pA as "$C_{3'}$-endo, $C_{4'}$-exo". There is a 15° difference in the dihedral angle about $C_{3'}$–$C_{4'}$ between this conformation and the accepted $C_{3'}$-endo conformation. However, the two conformers are sufficiently similar that the direction of the $O_{1'}$ effect on $H_{1'}$ can be determined and its magnitude estimated. The $H_{1'}$ of 1 m*M* <pA resonates at 6.227 ppm, whereas the average value of $H_{1'}$ of pA and Ap is 6.13 ppm (see footnote to Table I). Thus, when the furanose is frozen in the 3′-endo conformation the $H_{1'}$ is apparently deshielded by ~0.1 ppm. Though the magnitude of the effect is subject to considerable uncertainty, it does bring the measured and calculated $\Delta\delta_{duplex}$ values for the $H_{1'}$ resonances of A_2GCU_2 into closer agreement.

(*6*) *Effect of Minor Changes in the Glycosyl Angle,* χ_{CN}. In the oligonucleotide chain, the $H_{1'}$ atoms and bases are nearly coplanar in every residue when χ_{CN} is in the anti range. Thus, $H_{1'}$ is in a zone of fairly intense deshielding from the base. The effect of a 10–30° change in χ_{CN} from its average position in the mononucleotide to the duplex can probably account for about 0.10 ppm of the $\Delta\delta_{duplex}$ of $H_{1'}$ resonances observed in adenosine residues. The effect is much smaller, of course, for the other bases which do not have such intense ring currents.

(*7*) *Effect of the Phosphate.* Early in the discussion of the nature of chemical shifts of formation it was noted that H_8 and H_6 protons are shielded ~0.05 ppm more when the phosphate is diesterified than when it is monoesterified. Additionally, the P=O π-electron system is a potential source of magnetic anisotropy, in a manner analogous to the C=O situation. Both unesterified oxygens have double bond character in the internucleotidic phosphate. Therefore, the plane of maximal deshielding is expected to contain the phosphorus and both unesterified oxygen nuclei. (There is also a shielding zone above and below this plane.) ^1H NMR experiments on cyclic nucleotides give an indication of the size of the effect. Wechter (1969) published spectra of 2′,5′-cyclic arabinosylcytidylate, and a comparison with arabinosylcytosine showed that the $H_{3'}$ was deshielded ~1 ppm by the cyclic phosphodiester. Smith and Jardetzky (1968) published the ^1H NMR of 3′,5′-cyclic uridylate, and a comparison shows that $H_{4'}$ is deshielded by 0.27 ppm compared to uridine (Hruska et al., 1970). In both cases, an examination of molecular models shows that our expectations about the spatial distribution of the phosphate anisotropy are probably correct, and that the effect falls rapidly with distance. In examining the A_2GCU_2 spectra for phosphate effects, it is prudent to note that in the mononucleotides, which are the reference state for the shielding calculations, the phosphate is allowed free rotation. Thus, any anisotropic effect should be averaged out in the reference state. Limiting the conformational degrees of freedom, as in the duplex, may allow specific effects to be important. The nuclei of particular interest are $H_{1'}$, H_8, and H_6 as they are closest to the phosphate. The closest P–$H_{1'}$ radial distance in A′-RNA is ~5 Å and the $H_{1'}$ is nearly in the O–P–O plane, so the phosphate anisotropy is unlikely to be the source of the anomalously large $\Delta\delta_{duplex}$ values observed for the $H_{1'}$ protons. The closest radial distances for P–H_8 and P–H_6 are ~3.5 Å. This distance is close enough for the phosphate to exert an anisotropic effect. However, the orientation of H_8 and H_6 with respect to the O–P–O plane is about halfway between maximal shielding and maximal deshielding. Thus, it is likely that any component of $\Delta\delta_{duplex}$ for H_8 and H_6 due to the phosphate anisotropy is very small.

(*8*) *Effects of Deviations from Standard RNA Geometry.* It is obvious from the preceding discussion that there are many factors which influence the composite shielding effects on the protons in A_2GCU_2 upon helix formation. Even though the magnitude of the second-order effects discussed above could easily account for the discrepancies between measured and calculated shielding values, it remains very likely that the A′-RNA geometrical parameters are not strictly adhered to by every residue in the helical duplex. Minor changes in the tilt and twist angles or furanose conformation could certainly lead to magnetic effects as large as any of the second-order effects discussed above.

It is very important that a more exhaustive theoretical and empirical assessment of the above second-order effects be made. Only then can small chemical shift effects be properly associated with geometrical perturbations from standard geometries. Particularly the effects (5–7) that may strongly influence the $H_{1'}$ chemical shifts need to be evaluated. Careful NMR studies of model nucleotides with locked ribose conformations and locked conformations about the glycosidic bond are in order.

At present, the greatest usefulness of the chemical shifts of formation considered in the foregoing discussion is in comparative studies rather than the construction of a unique three-dimensional model. For instance, a comparative investigation with a short DNA helix of identical sequence would be of great value since some of the second-order effects would be nearly identical in such a comparison (such as hydrogen-bonding effects upon base pairing). Also, comparative NMR studies on the structural perturbations of these short helices by metal ions, intercalative drugs, etc., should be particularly amenable to conformational analysis at the atomic level.

Effects of Ionic strength and Position in the Helix on the Thermal Transition of the Chemical Shifts. The chemical shift vs. temperature profiles shown in Figure 7 contain

thermodynamic as well as structural information. These profiles are reports from 20 atoms at separate locations within the helix (including the three NH–N profiles) about their magnetic properties during the thermal transition; therefore in principle they can provide useful data to assign statistical weights to the various partially bonded states. However, each transition curve is a reflection of the changes in the *local* magnetic environment of each proton rather than a direct report on the helix–coil populations. In the partially formed duplex the δ value of a proton is determined by its δ value in each microstate, weighted according to the population of the state. Moreover, the value in a particular microstate is determined by shielding influences which are anisotropically distributed through space. Thus, in attempting to analyze the chemical shifts as a function of temperature, there are two variables to contend with: (1) the relative populations of the microstates and (2) the nonlinearity of the magnetic field effects in correlation to changes of the relative geometry of the atoms. The structural approach taken above depended on the selection of an experimental condition in which most of the molecules were frozen into one microstate, the helix, and then the chemical shifts of this microstate were analyzed for their geometrical content. This approach has been fruitful in a semiquantitative manner, but even so was hindered by the degeneracy of the shielding fields and the large number of shielding centers to be considered. When the population distribution is changed from narrow to broad, the situation obviously becomes much more complicated. The complexity of these effects is amply demonstrated by noting that protons within a single residue may have transition midpoints that differ by 10° or more (e.g., compare the T_m's in Table II for $G(3)H_8$ and $G(3)H_{1'}$ at identical ionic strengths). Also, the directions and magnitudes of the changes in chemical shift of protons on the same base may be greatly different. (For example, see the uridine H_5 and H_6 δ vs. T (°C) profiles in Figure 6.)

Faced with the difficulty of examining the nature of the structural transition on the microscopic scale, it is useful to try to detect general trends in the data. The first conclusion from this overall approach is that increasing the salt concentration increases helix stability as may be expected. More importantly, there appears to be no significant change in any of the individual transition breadths or limiting chemical shifts in either the helix state or the coil state at high temperature. This argues that basically the same helix and coil geometrical parameters persist over this range of ionic strength. The data argue against multiple aggregation of adjacent strands because one would expect the stability of such aggregates to have a stronger dependence on salt concentration than observed here (Record, 1967). An exception to the rule that the transition shapes are invariant with ionic strength are the $A(1)H_8$ profiles (Figure 6c). As the salt concentration is increased, this proton encounters substantially increased shielding. A similar, though smaller, effect is seen on $A(1)H_{1'}$; whether the effect is also exerted on $A(1)H_2$ is not clear. One explanation is that increasing the ionic strength stabilizes an end-to-end type of aggregation of colinear strands. Presumably these aggregates would be principally stabilized by the stacking properties of the adenine bases. The effect of salt would be to reduce polyelectrolyte effects and allow the ends of the two helices to come into contact. There are other plausible explanations, however. For instance, similar changes would be observed if increases in ionic strength stabilized the end bases against fraying or caused a general tightening of the helix. However, colinear aggregation better explains the degree of hypochromicity changes, resonance line broadening, and solubility changes than do the latter two hypotheses.

An average of the melting data in Table II has been found to compare favorably with optically determined T_m's (Figure 7). Thus, local environmental effects determining the shapes of the individual melting curves appear to be quite evenly distributed. While this overall average of T_m's corresponds to the overall helix–coil transition, averages of T_m's within each base pair reveal differences in relative stability of the three separate base pairs. The G·C pair is considerably more stable than the A·U pairs by this criterion. To say that the internal and terminal A·U pairs have equivalent stabilities is unwarranted because the A(1)·U(6) pair average covers only two protons. On the contrary, there is evidence from the NH–N resonances that the order of stability is A(1)·U(6) < A(2)·U(5) < G(3)·C(4) (Kan et al., 1975a).

Materials and Methods

Materials. Trisodium nucleoside 5′-diphosphates were purchased from Waldhof, Mannheim, W. Germany; ^{3}H-labeled nucleoside 5′-diphosphates from Schwarz/Mann, Orangeburg, N.Y.; Sephadex G-15, G-25 (coarse), and DEAE-Sephadex A-25 from Pharmacia, Piscataway, N.J.; Bio-Gel P-2 (50–100 mesh) and AG 501-X8 (D) (20–50 mesh) mixed bed resin from Bio-Rad, Richmond, Calif.; PEI-cellulose plates from Brinkmann, Westbury, N.Y.; RNase T_1 grade RT_1, RNase A grade RAF, and BAPase grade BAPC from Worthington, Freehold, N.J.; primer independent PNPase grade 0302 was from P-L Biochemicals, Milwaukee, Wis.; "Hy-Flo Super Cel" diatomaceous earth, "Norit A" activated charcoal, urea, and other miscellaneous chemicals were from Fisher Scientific, Pittsburgh, Pa.; "Spin-thimbles" were from Reeve-Angel, Clifton, N.J. All enzymatic reactions were carried out in plastic tubes, Falcon, Oxnard, Calif.; microliter volumes were transferred with Eppendorf pipets, Brinkmann, Westbury, N.Y. "Hydromix" (for aqueous samples) and "LSC Complete" (for papers and TLC strips) 2,5-diphenyloxazole-1,4-bis[2-(5-phenyloxazolyl)]benzene liquid scintillation cocktails were purchased from Yorktown Research, New Hyde Park, N.Y. Special uv absorbance cells were purchased from Pyrocell, Westwood, N.J.

Instrumentation. Uv absorbance measurements were made on a Cary 14 or Cary 15 spectrophotometer. Absorbance–temperature profiles were recorded on the Cary 15 equipped with the standard Cary thermojacketed cell holder. Temperature was regulated by a Haake KT-62 circulating bath and recorded by a YSI telethermometer with its thermostat embedded in the cell holder. The cuvets for recording uv absorbance at 10 mM C_s were similar to those described in Borer et al. (1974b) with these exceptions: the path length of the cell was 2 mm and the insert was 1.98 mm thick. This resulted in a nominal 0.002-cm path length. The actual path length was calibrated with respect to a 1.000-cm path-length cell by measuring the absorbance of a 50 mM Up solution in the 0.002-cm path, diluting 500-fold, and measuring in the 1.000-cm cell. It was also found that the path length changed appreciably and reproducibly as a function of temperature. This factor was corrected in the reported A_{260} vs. T profiles for the oligomers. These profiles were reproducible and showed no evidence of appreciable evaporation or hysteresis of melting.

Radioactive samples were counted on a Beckmann LS-200B liquid scintillation counter.

Proton Magnetic Resonance. Samples were lyophilized three or more times in 99.8% D_2O, 0.01 *M* sodium phosphate (pD 7.0) buffer, 10^{-4} *M* EDTA, with NaCl added to a final Na^+ concentration of 0.07 *M* (10 m*M* $Na_5A_2GCU_2$, no added NaCl), 0.17 *M* (10 m*M* $Na_5A_2GCU_2$, 0.1 *M* NaCl added), or 1.07 *M* (10 m*M* $Na_5A_2GCU_2$, 1 *M* NaCl added) in a final volume of 0.40 ml. The A_2GCU_2 concentration was determined by measuring A_{260} in very dilute ($C_s \simeq 10^{-5}$ *M*) solution at 25°C in the absence of salt. The extinction coefficient used for A_2GCU_2 is 61.8 A_{260} units/μmol strand under these conditions. This value was calculated on the basis of the nearest-neighbor approximation (Warshaw and Tinoco, 1966).

The proton magnetic resonance spectra were recorded on a Varian HA-100 or a Varian HR-220 spectrometer operating in the frequency mode by use of the Fourier transform free induction decay technique. The Varian HA-100 was equipped with a Digilab pulse unit and a Data General Nova computer; and the HR-220 was equipped with a Varian 620i computer, V4357 pulse unit, and RF amplifier. Chemical shifts were measured from an internal standard of *t*-butyl alcohol but reported in reference to DSS as shown in the following equation:

$$\delta_{DSS} = \delta_{t\text{-BuOH}} + 1.244 - 0.00015T$$

where δ_{DSS} and $\delta_{t\text{-BuOH}}$ are the chemical shifts with respect to DSS and *t*-butyl alcohol in that order, and T is the temperature in °C. Probe temperatures of the HA-100 and HR-220 were regulated by a Varian 6507 or a Varian 4257 variable temperature accessory, respectively, and monitored by observing the splitting in methanol and ethylene glycol. Temperature control was accurate to ±1°C. For narrow resonance signals, the relative spectral positions are accurate to ±0.002 ppm within a given spectrum and to ±0.005 ppm among different spectral measurements.

Synthesis. The synthesis of A_2GCU_2 closely follows previously published procedures: Uhlenbeck et al. (1971), Gralla and Crothers (1973a), Borer et al. (1973), and is briefly outlined in Chart I. A disadvantage of the earlier procedures is that they were developed for syntheses on a 10–100-μg scale and depend heavily on paper chromatographic purifications. However, the methods summarized below and detailed in the microfilm edition of this journal contain innovations which allow the facile synthesis of oligomers on the 50-mg scale and are readily adaptable to larger syntheses. Also, the standard techniques are presented in greater detail than ever before in order that they may be exploited more easily by other workers.

Chart I: Synthesis of ApApGpCpU*pU*.[a]

	Yield (%)
1. ppA + ppG $\xrightarrow{\text{PNPase}}$ poly(A,G) (input ratio 3A:1G)	54
2. poly(A,G) $\xrightarrow{\text{RNase } T_1}$ A_nG_p $\xrightarrow{\text{DEAE-Seph}}$ A_2Gp $\xrightarrow[\text{Seph G-15}]{\text{BAPase}}$ A_2G	15
3. A_2G + ppC $\xrightarrow[\text{RNase A}]{\text{PD PNPase}}$ A_2GCP $\xrightarrow[\text{Seph G-25}]{\text{BAPase, DEAE-Seph}}$ A_2GC	45
4. A_2GC + ppU* $\xrightarrow{\text{PD PNPase}}$ $A_2GCU^*_n$ $\xrightarrow[\text{Bio-Gel P-2}]{\text{DEAE-Seph}}$ $A_2GCU^*_2$	43

[a] U* = ^{3}H-labeled uridine at 25 μCi/mmol.

Preparation of A_2G. ADP and GDP were copolymerized with PNPase to produce poly(A,G). The enzyme and unpolymerized diphosphates were removed and the polymer was hydrolyzed with RNase T_1. The resulting A_nGp oligomers were then separated on a DEAE-Sephadex-Cl^- anion exchange column with a linear NaCl gradient in 7 *M* urea. The A_2Gp peak was desalted by loading on a small DEAE-Seph-HCO_3^- column, eluting with 1 *M* TEA-HCO_3, and stripping off the solvent and salt under vacuum. The terminal phosphate was removed with BAPase and A_2G was separated from enzymes and inorganic phosphate on a Sephadex G-15 column. (It was discovered in a later step that this procedure left traces of RNase T_1 in the A_2G.)

Preparation of A_2GC. A single cytidylate was esterified to the 3′-OH of A_2G in the presence of primer-dependent PNPase and RNase A. The terminal phosphate of the A_2GCp produced was removed with BAPase and the products were purified on DEAE-Seph-HCO_3^- with a linear gradient in TEA-HCO_3. The presence of a considerable amount of $A_2Gp>$ in this elution profile indicated a contamination with RNase T_1 in the reaction mixture. A_2GC was separated from contaminating enzymes on a Sephadex G-25 column in 7 *M* urea–0.05 *M* NaCl. The sample was desalted as above on a small DEAE-Seph-HCO_3^- column.

Preparation of A_2GCU_2. A_2GC and UDP were copolymerized in the presence of PD PNPase to form a series of A_2GCU_n oligomers. The time, enzyme, and solution conditions were carefully determined in small scale trial reactions to optimize the yield of A_2GCU_2. Phosphorolysis was suppressed by using a high ratio of UDP/A_2GC (= 22/1). The products were separated on DEAE-Seph-Cl^- with a linear NaCl gradient in 7 *M* urea. Desired oligomer peaks were purified from urea and concentrated on small DEAE-Seph-Cl^- columns and eluted with 1 *M* NaCl. They were then desalted on Bio-Gel P-2 columns until salt free. This purification procedure resulted in the production of oligomers directly usable for high-resolution NMR analysis. It was necessary to add only 10^{-4} *M* EDTA to sharpen the lines broadened by paramagnetic ions, and the oligomers are in the Na^+ form with no TEA^+ contamination. A total of 35 mg of A_2GCU_2 was prepared.

Proof of Sequence. The sequence integrity of the oligomeric products and intermediates was carefully checked after each synthetic step. This involved alkaline hydrolysis and determination of base ratios for several early peaks from the A_nG_p column. The mobilities and uv spectra of these digestion products as well as the parent oligomers were compared with authentic marker compounds on paper chromatography. Base ratios and RNase T_1 digestion products were also analyzed for the products of the A_2G + CDP reaction. Additional support for their identity was generated by an analysis of their ^{1}H NMR spectra. The proof of the A_2GCU_2 sequence is outlined in Chart II. Of course, if the sequence can be proven at this level, the identification of the intermediate oligomers is rather superfluous. However, some of the proof relies on separation paper chromatography which did not always completely resolve the components. Also quantitation of nucleotides from paper by their uv spectra is subject to errors on the order of 10–20% due to difficulties with nonuniform background absorbance from the paper. Therefore, it is noteworthy that the sequencing results for the intermediates also support the A_2GCU_2 sequence.

In the final synthetic step, UDP was lightly labeled with ^{3}H (Chart I). Therefore, the products separated on the

Chart II: Identification of ApApGpCpUp*U*.[a]

1. Ratio of radioactivity of column fractions $A_2GCU^*_2/A_2GCU^* = 2.1 \pm 0.1$	
2a. $A_2GCU^*_2 \xrightarrow{\text{RNase } T_1} X + Y^*$	$X/Y^* = 0.98 \pm 0.1$[b]
b. $X \xrightarrow{OH^-} Ap + Gp$	$Ap/Gp = 1.8/1.0 \pm 0.2$
c. $Y^* \xrightarrow{OH^-} Cp + U^*p + U^*$	
3a. $A_2GCU^*_2 \xrightarrow{\text{RNase A}} Z + U^*p + U^*$	$U^*_p/U^* = 0.94/1.00 \pm 0.05$
b. $Z \xrightarrow{OH^-} Ap + Gp + Cp$	$Ap/Gp/Cp = 1.9/1.0/0.8 \pm 0.2$
4. $A_2GCU^*_2 \xrightarrow{OH^-} Ap + Gp + Cp + U^*p + U^*$	$U^*p/U^* = 1.05/1.00 \pm 0.05$

[a] U* = ^{3}H-labeled uridine at 25 μCi/mmol. [b] This ratio is based on their uv spectra and that X = AAGp with $\epsilon_{260} = 37.0\ A_{260}$ units/μmol, and Y* = CUU with $\epsilon_{260} = 25.9\ A_{260}$ units/μmol. (Extinction coefficient values are calculated from the dinucleoside monophosphate absorbance values of Warshaw and Tinoco (1966).)

anion exchange column could be tentatively identified by the ratio of their specific activities (Chart II-1). The RNase T_1 and RNase A digestion products of the hexamer were separated by 2 kV electrophoresis at pH 3.5 (pyridinium acetate buffer 0.05 *M*) on DEAE paper. After drying the paper, rinsing in ethyl acetate, and illuminating with a uv light only the products indicated in Chart II were observed. Spots X, Y*, and Z were eluted with 2 *M* TEA-HCO_3, dried, and further hydrolyzed with 0.3 *M* NaOH. The identity of the products of the hydrolysis and their stoichiometry were determined by descending chromatography on Whatman 3MM paper in solvent 70 E (95% ethanol–1 *M* ammonium acetate = 7:3). The spots were eluted with water and their uv absorbance was measured. In order to determine U*p/U* ratios, it was necessary to eliminate washing with ethyl acetate because some of the nucleoside washed off the paper. This precluded electrophoresis in pyridine buffers, so the RNase A hydrolysis (Chart II-3a) was repeated and the alkaline hydrolysis (II-4) products were separated on paper in solvent 70 E. The spots were eluted with 1 ml of H_2O and counted in a "Hydromix" scintillation cocktail.

These results completely and redundantly support the integrity of the sequence A_2GCU_2. Particularly the result that two and only two products result from reaction 2a imply a purity of product ≥95%. Furthermore, the ^{1}H NMR spectra in Figures 1 and 2 show no unaccountable peaks. It is obvious that only the most subtle of impurities could escape a 5% detection limit in these spectra.

Acknowledgments

We thank Drs. J. L. Alderfer, D. W. Cochran, and D. M. Crothers for helpful discussions, and Dr. B. Pullman for providing many useful unpublished ring current isoshielding contours.

Supplementary Material Available

Further material relevant to the synthesis of A_2GCU_2 will appear following these pages in the microfilm edition of this volume of the journal. Photocopies of the supplementary material from this paper only or microfiche (105 × 148 mm, 24× reduction, negatives) containing all of the supplementary material for the papers in this issue may be obtained from the Business Office, Books and Journals Division, American Chemical Society, 1155 16th St., N.W., Washington, D.C. 20036. Remit check or money order for $4.50 for photocopy or $2.50 for microfiche, referring to code number BIO-75-4847.

References

Alderfer, J. L., and Smith, S. L. (1971), *J. Am. Chem. Soc. 93,* 7305.

Alderfer, J. L., Tazawa, I., Tazawa, S., and Ts'o, P. O. P. (1974), *Biochemistry 13,* 1615.

Arnott, S., and Hukins, D. W. L. (1972), *Biochem. Biophys. Res. Commun. 47,* 1504.

Arnott, S., and Hukins, D. W. L. (1973), *J. Mol. Biol. 81,* 93.

Arnott, S., Hukins, D. W. L., and Dover, S. D. (1972), *Biochem. Biophys. Res. Commun. 48,* 1392.

Arnott, S., Hukins, D. W. L., Dover, S. D., Fuller, W., and Hodgson, A. R. (1973), *J. Mol. Biol. 81,* 107.

Arter, D. B., Walker, G. C., Uhlenbeck, O. C., and Schmidt, P. G. (1974), *Biochem. Biophys. Res. Commun. 61,* 1089.

Borer, P. N., Alderfer, J., Kan, L. S., Leutzinger, E. E., and Ts'o, P. O. P. (1974a), *Fed. Proc., Fed. Am. Soc. Exp. Biol. 33,* 1537.

Borer, P. N., Dengler, B., Tinoco, Jr., I., and Uhlenbeck, O. C. (1974b), *J. Mol. Biol. 86,* 843.

Borer, P. N., Uhlenbeck, O. C., Dengler, B., and Tinoco, Jr., I. (1973), *J. Mol. Biol. 80,* 759.

Bovey, F. A. (1969), *Nuclear Magnetic Resonance Spectroscopy,* New York, N.Y., Academic Press.

Craig, M. E., Crothers, D. M., and Doty, P. (1971), *J. Mol. Biol. 62,* 383.

Cross, A. D., and Crothers, D. M. (1971), *Biochemistry 10,* 4015.

Day, R. O., Seeman, N. C., Rosenberg, J. M., and Rich, A. (1973), *Proc. Natl. Acad. Sci. U.S.A. 70,* 849.

Giessner-Prettre, C., and Pullman, B. (1970a), *J. Theor. Biol. 27,* 87.

Giessner-Prettre, C., and Pullman, B. (1970b), *C. R. Hebd. Seances Acad. Sci., Ser. A, 270,* 866.

Gralla, J., and Crothers, D. M. (1973a), *J. Mol. Biol. 73,* 497.

Gralla, J., and Crothers, D. M. (1973b), *J. Mol. Biol. 78,* 301.

Heller, M. J., Tu, A. T., and Maciel, G. E. (1974), *Biochemistry 13,* 1623.

Hruska, F. E., Bell, C. L., Victor, T. A., and Danyluk, S. S. (1968), *Biochemistry 7,* 3721.

Hruska, F. E., and Danyluk, S. S. (1968), *J. Am. Chem. Soc. 90,* 3266.

Hruska, F. E., Grey, A. A., and Smith, I. C. P. (1970), *J. Am. Chem. Soc. 92,* 4088.

Johnson, C. E., and Bovey, F. A. (1958), *J. Chem. Phys. 29,* 1012.

Kan, L. S., Borer, P. N., and Ts'o, P. O. P. (1975a), *Biochemistry,* following paper in this issue.

Kan, L. S., Borer, P. N., and Ts'o, P. O. P. (1975b), 169th Abstracts, National Meeting of the American Chemical Society, Philadelphia, Pa., No. MEDI-29.

Katz, L. (1969), *J. Mol. Biol. 44,* 279.

Katz, L., and Penman, S. (1966), *J. Mol. Biol. 15,* 220.

Kondo, N. S., and Danyluk, S. S. (1972), *J. Am. Chem. Soc. 94,* 5121.

Kondo, N. S., Fang, K. N., Miller, P. S., and Ts'o, P. O. P. (1972), *Biochemistry 11,* 1991.

Kreishman, G. P., and Chan, S. I. (1971), *Biopolymers 10,* 159.

Lubas, B., and Wilczok, T. (1971), *Biopolymers 10,* 1267.
McDonald, C. C., Phillips, W. D., and Lazar, J. (1967), *J. Am. Chem. Soc. 89,* 4166.
McDonald, C. C., Phillips, W. D., and Penman, S. (1964), *Science 144,* 1234.
McTague, J. P., Ross, V., and Gibbs, J. H. (1964), *Biopolymers 2,* 163.
Martin, F. H., Uhlenbeck, O. C., and Doty, P. (1971), *J. Mol. Biol. 57,* 201.
Newmark, R. A., and Cantor, C. R. (1968), *J. Am. Chem. Soc. 90,* 5010.
Patel, D. J., and Tonelli, A. (1974), *Biopolymers 13,* 1943.
Pörschke, D., Uhlenbeck, O. C., and Martin, F. H. (1973), *Biopolymers 12,* 1313.
Ravetch, J., Gralla, J., and Crothers, D. M. (1974), *Nucleic Acids Res. 1,* 109.
Record, M. T. (1967), *Biopolymers 5,* 975.
Rosenberg, J. M., Seeman, N. C., Kim, J. J. P., Suddath, F. L., Nicholas, H. G., and Rich, A. (1973), *Nature (London) 243,* 150.
Shoup, R. R., Miles, H. T., and Becker, E. D. (1966), *Biochem. Biophys. Res. Commun. 23,* 194.
Smith, M., and Jardetzky, C. D. (1968), *J. Mol. Spectrosc. 28,* 70.
Ts'o, P. O. P. (1974a), *Basic Principles in Nucleic Acid Chemistry,* Vol. I, New York, N.Y., Academic Press, p 453.
Ts'o, P. O. P. (1974b), *Basic Principles in Nucleic Acid Chemistry,* Vol. II, New York, N.Y., Academic Press, p 305.
Ts'o, P. O. P., Alderfer, J. L., Borer, P. N., and Kan, L. S. (1975), Proceedings of the Steenbock Symposium (in press).
Ts'o, P. O. P., Barrett, J. C., Kan, L. S., and Miller, P. S. (1973), *Ann. N.Y. Acad. Sci. 222,* 290.
Ts'o, P. O. P., Kondo, N. S., Robins, R. K., and Broom, A. D. (1969), *J. Am. Chem. Soc. 91,* 5625.
Uhlenbeck, O. C., Martin, F. H., and Doty, P. (1971), *J. Mol. Biol. 57,* 217.
Warshaw, M. M., and Tinoco, Jr., I. (1966), *J. Mol. Biol. 20,* 29.
Waugh, J. S., and Fessenden, R. W. (1957), *J. Am. Chem. Soc. 79,* 846.
Wechter, W. J. (1969), *J. Org. Chem. 34,* 244.